Heat Transfer Engineering, 31(9):711–732, 2010

ISSN: 0145-7632 print / 1521-0537 online
DOI: 10.1080/01457630903500833

Taylor & Francis
Taylor & Francis Group

Importance of Non-Boiling Two-Phase Flow Heat Transfer in Pipes for Industrial Applications

AFSHIN J. GHAJAR and CLEMENT C. TANG

School of Mechanical and Aerospace Engineering, Oklahoma State University, Stillwater, Oklahoma, USA

The validity and limitations of the numerous two-phase non-boiling heat transfer correlations that have been published in the literature over the past 50 years are discussed. The extensive results of the recent developments in the non-boiling two-phase heat transfer in air–water flow in horizontal and inclined pipes conducted at Oklahoma State University's two-phase flow heat transfer laboratory are presented. Practical heat transfer correlations for a variety of gas–liquid flow patterns and pipe inclination angles are recommended. The application of these correlations in engineering practice and how they can influence the equipment design and consequently the process design are discussed.

INTRODUCTION

In many industrial applications, such as the flow of oil and natural gas in flow lines and well bores, the knowledge of non-boiling two-phase, two-component (liquid and permanent gas) heat transfer is required. During the production of two-phase hydrocarbon fluids from an oil reservoir to the surface, the temperature of the hydrocarbon fluids changes due to the difference in temperatures of the oil reservoir and the surface. The change in temperature results in heat transfer between the hydrocarbon fluids and the earth surrounding the oil well, and the ability to estimate the flowing temperature profile is necessary to address several design problems in petroleum production engineering [1].

In subsea oil and natural gas production, hydrocarbon fluids may leave the reservoir with a temperature of 75°C and flow in subsea surrounding of 4°C [2]. As a result of the temperature gradient between the reservoir and the surrounding, the knowledge of heat transfer is critical to prevent gas hydrate and wax deposition blockages [3]. Wax deposition can result in problems, including reduction of inner pipe diameter causing blockage, increased surface roughness of pipe leading to restricted flow line pressure, decrease in production, and various mechanical problems [4]. Some examples of the economical losses caused by the wax deposition blockages include: direct cost of removing the blockage from a subsea pipeline was $5 million, production downtime loss in 40 days was $25 million [5], and the cost of oil platform abandonment by Lasmo Company (UK) was $100 million [6].

In situations where low-velocity flow is necessary while high heat transfer rates are desirable, heat transfer enhancement schemes such as the coil-spring wire insert, twisted tape insert, and helical ribs are used to promote turbulence, thus enhancing heat transfer. Although these heat transfer enhancement schemes have been proven to be effective, they do come with drawbacks, such as fouling, increase in pressure drop, and sometimes even blockage. Celata et al. [7] presented an alternative approach to enhance heat transfer in pipe flow, by injecting gas into liquid to promote turbulence. In the experimental study performed by Celata et al. [7], a uniformly heated vertical pipe was internally cooled by water, while heat transfer coefficients with and without air injection were measured. The introduction of low air flow rate into the water flow resulted in increase of the heat transfer coefficient up to 20–40% for forced convection, and even larger heat transfer enhancement for mixed convection [7].

This is an extended version of the keynote paper presented at the 11th Conference on Process Integration, Modeling and Optimization for Energy Saving and Pollution Reduction (PRES2008), Prague, Czech Republic, August 24–28, 2008.

Generous contributions in equipment and software made by National Instruments are gratefully acknowledged. Sincere thanks are offered to Micro Motion for generously donating one of the Coriolis flow meters and providing a substantial discount on the other one. Thanks are also due to Martin Mabry for his assistance in procuring these meters.

Address correspondence to Professor Afshin J. Ghajar, School of Mechanical and Aerospace Engineering, Oklahoma State University, Stillwater, OK 74078, USA. E-mail: afshin.ghajar@okstate.edu

Two-phase flow can also occur in various situations related to ongoing and planned space operations, and the understanding of heat transfer characteristics is important for designing piping systems for space operations limited by size constraints [8]. To investigate heat transfer in two-phase slug and annular flows under reduced gravity conditions, Fore et al. [8, 9] conducted heat transfer measurements for air–water and air–50% aqueous glycerin aboard NASA's Zero-G KC-135 aircraft.

Due to limited studies available in the literature, Wang et al. [10] investigated forced convection heat transfer on the shell side of a TEMA-F horizontal heat exchanger using a 60% aqueous glycerin and air mixture. Their work resulted in recommendation of correlations for two-phase heat transfer coefficient in stratified, intermittent, and annular flows in shell-and-tube heat exchangers.

In this article, an overview of our ongoing research on this topic that has been conducted at our heat transfer laboratory over the past several years is presented. Our extensive literature search revealed that numerous heat transfer coefficient correlations have been published over the past 50 years. We also found several experimental data sets for forced convective heat transfer during gas–liquid two-phase flow in vertical pipes, very limited data for horizontal pipes, and no data for inclined pipes. However, the available correlations for two-phase convective heat transfer were developed based on limited experimental data and are only applicable to certain flow patterns and fluid combinations.

The overall objective of our research has been to develop a heat transfer correlation that is robust enough to span all or most of the fluid combinations, flow patterns, flow regimes, and pipe orientations (vertical, inclined, and horizontal). To this end, we have constructed a state-of-the-art experimental facility for systematic heat transfer data collection in horizontal and inclined positions (up to 7°). The experimental setup is also capable of producing a variety of flow patterns and is equipped with two transparent sections at the inlet and exit of the test section for in-depth flow visualization. In this article we present the highlights of our extensive literature search, the development of our proposed heat transfer correlation and its application to experimental data in horizontal, inclined, and vertical pipes, a detailed description of our experimental setup, the flow visualization results for different flow patterns, the experimental results for various flow patterns, and our proposed heat transfer correlation for various flow patterns and pipe orientations.

COMPARISON OF 20 TWO-PHASE HEAT TRANSFER CORRELATIONS WITH SEVEN SETS OF EXPERIMENTAL DATA

Numerous heat transfer correlations and experimental data for forced convective heat transfer during gas–liquid two-phase flow in vertical and horizontal pipes have been published over the past 50 years. In a study published by Kim et al. [11], a comprehensive literature search was carried out and a total of 38 two-phase flow heat transfer correlations were identified. The validity of these correlations and their ranges of applicability have been documented by the original authors. In most cases, the identified heat transfer correlations were based on a small set of experimental data with a limited range of variables and gas–liquid combinations. In order to assess the validity of those correlations, they were compared against seven extensive sets of two-phase flow heat transfer experimental data available from the literature, for vertical and horizontal tubes and different flow patterns and fluids. For consistency, the validity of the identified heat transfer correlations were based on the comparison between the predicted and experimental two-phase heat transfer coefficients meeting the ±30% criterion.

In total, 524 data points from the five available experimental studies [12–16] were used for these comparisons (see Table 1). The experimental data included five different gas–liquid combinations (air–water, air–glycerin, air–silicone, helium–water, Freon 12–water), and covered a wide range of variables, including liquid and gas flow rates and properties, flow patterns, pipe sizes, and pipe inclination. Five of these experimental data sets are concerned with a wide variety of flow patterns in vertical pipes and the other two data sets are for limited flow patterns (slug and annular) within horizontal pipes.

Table 2 shows 20 of the 38 heat transfer correlations [14, 16–35] that were identified and reported by Kim et al. [11]. Eighteen of the two-phase flow heat transfer correlations were not tested, since the required information for those correlations was not available through the identified experimental studies. In assessing the ability of the 20 identified heat transfer correlations, their predictions were compared with the experimental data from the sources listed in Table 1, both with and without considering the restrictions on Re_{SL} and V_{SG}/V_{SL} accompanying the correlations. The results from comparing the 20 heat transfer correlations and the experimental data are summarized in Table 3 for major flow patterns in vertical pipes.

There were no remarkable differences for the recommendations of the heat transfer correlations based on the results with and without the restrictions on Re_{SL} and V_{SG}/V_{SL}, except for the correlations of Chu and Jones [18] and Ravipudi and Godbold [25], as applied to the air–water experimental data of Vijay [12]. Details of this discussion can be found in Kim et al. [11].

Based on the results without the authors' restrictions on Re_{SL} and V_{SG}/V_{SL}, the correlation of Chu and Jones [18] was

Table 1 The experimental data used in Kim et al. [11]

Source	Orientation	Fluids	Number of data points
Vijay [12]	Vertical	Air–water	139
Vijay [12]	Vertical	Air–glycerin	57
Rezkallah [13]	Vertical	Air–silicone	162
Aggour [14]	Vertical	Helium–water	53
Aggour [14]	Vertical	Freon 12–water	44
Pletcher [15]	Horizontal	Air–water	48
King [16]	Horizontal	Air–water	21

Table 2 Heat transfer correlations chosen by Kim et al. [11]

Source	Heat transfer correlations	Source	Heat transfer correlations
Aggour [14]	$h_{TP}/h_L = (1-\alpha)^{-1/3}$ Laminar (L) $Nu_L = 1.615(Re_{SL}Pr_L D/L)^{1/3}(\mu_B/\mu_W)^{0.14}$ (L) $h_{TP}/h_L = (1-\alpha)^{-0.83}$ Turbulent (T) $Nu_L = 0.0155Re_{SL}^{0.83}Pr_L^{0.5}(\mu_B/\mu_W)^{0.33}$ (T)	Knott et al. [17]	$\frac{h_{TP}}{h_L} = \left(1+\frac{V_{SG}}{V_{SL}}\right)^{1/3}$ where h_L is from Sieder and Tate [35]
Chu and Jones [18]	$Nu_{TP} = 0.43(Re_{TP})^{0.55}(Pr_L)^{1/3}\left(\frac{\mu_B}{\mu_W}\right)^{0.14}\left(\frac{Pa}{P}\right)^{0.17}$	Kudirka et al. [19]	$Nu_{TP} = 125\left(\frac{V_{SG}}{V_{SL}}\right)^{1/8}\left(\frac{\mu_G}{\mu_L}\right)^{0.6}(Re_{SL})^{1/4}(Pr_L)^{1/3}\left(\frac{\mu_B}{\mu_W}\right)^{0.14}$
Davis and David [20]	$Nu_{TP} = 0.060\left(\rho_L/\rho_G\right)^{0.28}\left(DG_i x/\mu_L\right)^{0.87}Pr_L^{0.4}$	Martin & Sims [21]	$h_{TP}/h_L = 1+0.64\sqrt{V_{SG}/V_{SL}}$ where h_L is from Sieder and Tate [35]
Dorresteijn [22]	$h_{TP}/h_L = (1-\alpha)^{-1/3}$ (L) $h_{TP}/h_L = (1-\alpha)^{-0.8}$ (T) $Nu_L = 0.0123Re_{SL}^{0.9}Pr_L^{0.33}(\mu_B/\mu_W)^{0.14}$	Oliver and Wright [23]	$Nu_{TP} = Nu_L\left(\frac{1.2}{R_L^{0.36}} - \frac{0.2}{R_L}\right)$ $Nu_L = 1.615\left[\frac{(Q_G+Q_L)\rho D}{A\mu}Pr_L\, D/L\right]^{1/3}(\mu_B/\mu_W)^{0.14}$
Dusseau [24]	$Nu_{TP} = 0.029(Re_{TP})^{0.87}(Pr_L)^{0.4}$	Ravipudi and Godbold [25]	$Nu_{TP} = 0.56\left(\frac{V_{SG}}{V_{SL}}\right)^{0.3}\left(\frac{\mu_G}{\mu_L}\right)^{0.2}(Re_{SL})^{0.6}(Pr_L)^{1/3}\left(\frac{\mu_B}{\mu_W}\right)^{0.14}$
Elamvaluthi and Srinivas [26]	$Nu_{TP} = 0.5\left(\mu_G/\mu_L\right)^{1/4}(Re_{TP})^{0.7}(Pr_L)^{1/3}\left(\mu_B/\mu_W\right)^{0.14}$	Rezkallah and Sims [27]	$h_{TP}/h_L = (1-\alpha)^{-0.9}$ where h_L is from Sieder and Tate [35]
Groothuis and Hendal [28]	$Nu_{TP} = 0.029(Re_{TP})^{0.87}(Pr_L)^{1/3}(\mu_B/\mu_W)^{0.14}$ (for air–water) $Nu_{TP} = 2.6(Re_{TP})^{0.39}(Pr_L)^{1/3}(\mu_B/\mu_W)^{0.14}$ (for air–(gas–oil))	Serizawa et al. [29]	$\frac{h_{TP}}{h_L} = 1+462X_{TT}^{-1.27}$ where h_L is from Sieder and Tate [35]
Hughmark [30]	$Nu_{TP} = 1.75\,(R_L)^{-1/2}\left(\frac{\dot{m}_L c_L}{R_L k_L L}\right)^{1/3}\left(\frac{\mu_B}{\mu_W}\right)^{0.14}$	Shah [31]	$h_{TP}/h_L = \left(1+V_{SG}/V_{SL}\right)^{1/4}$ $Nu_L = 1.86(Re_{SL}\, Pr_L\, D/L)^{1/3}(\mu_B/\mu_W)^{0.14}$ (L) $Nu_L = 0.023Re_{SL}^{0.8}Pr_L^{0.4}\left(\mu_B/\mu_W\right)^{0.14}$ (T)
Khoze et al. [32]	$Nu_{TP} = 0.26\,Re_{SG}^{0.2}Re_{SL}^{0.55}Pr_L^{0.4}$	Ueda and Hanaoka [33]	$Nu_{TP} = 0.075(Re_M)^{0.6}\frac{Pr_L}{1+0.035(Pr_L-1)}$
King [16]	$\frac{h_{TP}}{h_L} = \frac{R_L^{-0.52}}{1+0.025Re_{SG}^{0.5}}\left[\left(\frac{\Delta P}{\Delta L}\right)_{TP}\Big/\left(\frac{\Delta P}{\Delta L}\right)_L\right]^{0.32}$ $Nu_L = 0.023Re_{SL}^{0.8}Pr_L^{0.4}$	Vijay et al. [34]	$h_{TP}/h_L = (\Delta P_{TPF}/\Delta P_L)^{0.451}$ $Nu_L = 1.615(Re_{SL}Pr_L\, D/L)^{1/3}(\mu_B/\mu_W)^{0.14}$ (L) $Nu_L = 0.0155Re_{SL}^{0.83}Pr_L^{0.5}(\mu_B/\mu_W)^{0.33}$ (T)
		Sieder and Tate [35]	$Nu_L = 1.86(Re_{SL}\, Pr_L\, D/L)^{1/3}(\mu_B/\mu_W)^{0.14}$ (L) $Nu_L = 0.027Re_{SL}^{0.8}Pr_L^{0.33}(\mu_B/\mu_W)^{0.14}$ (T)

Note. α and R_L are taken from the original experimental data. $Re_{SL} < 2000$ implies laminar flow, otherwise turbulent; and for Shah [31], replace 2000 by 170. With regard to the equations given for Shah [31] in this table, the laminar two-phase correlation was used along with the appropriate single-phase correlation, since Shah [31] recommended a graphical turbulent two-phase correlation.

Table 3 Recommended correlations for vertical pipes, Kim et al. [11]

	Air–water				Air–glycerin				Air–silicone					Helium–water				Freon 12–water				Air–water	
Correlations	B	S	F	A	B	S	F	A	B	S	C	A	F	B	S	F	A	B	S	F	A	A	S
Aggour [14]	√	√			√	√	√	√										√	√	√	√		
Chu and Jones [18]				√										√		√				√			√
Knott et al. [17]			√										√	√	√	√		√		√			
Kudirka et al. [19]																							√
Martin and Sims [21]	√													√				√	√	√	√		√
Ravipudi and Godbold [25]				√							√	√							√				√
Rezkallah and Sims [27]	√								√	√	√			√				√	√	√	√		
Shah [31]	√		√		√				√				√	√		√		√		√		√	

Note. √ = Recommended correlation with and without restrictions. Shaded cells indicate the correlations that best satisfied the ±30% two-phase heat transfer coefficient criterion. A = annular, B = bubbly, C = churn, F = froth, S = slug.

recommended for only annular, bubbly-froth, slug-annular, and froth-annular flow patterns of air–water in vertical pipes. While the correlation of Ravipudi and Godbold [25] was recommended for only annular, slug-annular, and froth-annular flow patterns of air–water in vertical pipes.

However, when considering the Re_{SL} and V_{SG}/V_{SL} restrictions by the authors, the correlation of Chu and Jones [18] was recommended for all vertical pipe air–water flow patterns including transitional flow patterns, except the annular-mist flow pattern. While the correlation of Ravipudi and Godbold [25] was recommended for slug, froth, and annular flow patterns and for all of the transitional flow patterns of the vertical air–water experimental data.

All of the correlations just recommended have the following important parameters in common: Re_{SL}, Pr_L, μ_B/μ_W, and either void fraction (α) or superficial velocity ratio (V_{SG}/V_{SL}). It appears that void fraction and superficial velocity ratio, although not directly related, may serve the same function in two-phase flow heat transfer correlations.

From the comprehensive literature search, Kim et al. [11] found that there is no single correlation capable of predicting the flow for all fluid combinations in vertical pipes. In the following section, the effort of Kim et al. [36] in developing a heat transfer correlation that is robust enough to span all or most of the fluid combinations and flow patterns for vertical pipes is highlighted.

Kim et al. [36] developed a correlation that is capable of predicting heat transfer coefficient in two-phase flow regardless of fluid combinations and flow patterns. The correlation uses a carefully derived heat transfer model that takes into account the appropriate contributions of both the liquid and gas phases using the respective cross-sectional areas occupied by the two phases.

DEVELOPMENT OF THE HEAT TRANSFER CORRELATION FOR VERTICAL PIPES

The void fraction (α) is defined as the ratio of the gas-flow cross-sectional area (A_G) to the total cross-sectional area, A ($= A_G + A_L$):

$$\alpha = \frac{A_G}{A_G + A_L} \tag{1}$$

The actual gas velocity V_G can be calculated from

$$V_G = \frac{Q_G}{A_G} = \frac{\dot{m}_G}{\rho_G A_G} = \frac{\dot{m}x}{\rho_G \alpha A} \tag{2}$$

Similarly, for the liquid, V_L is defined as:

$$V_L = \frac{Q_L}{A_L} = \frac{\dot{m}_L}{\rho_L A_L} = \frac{\dot{m}(1-x)}{\rho_L (1-\alpha) A} \tag{3}$$

The total gas–liquid two-phase heat transfer coefficient is assumed to be the sum of the individual single-phase heat transfer coefficients of the gas and liquid phases, weighted by the volume of each phase present:

$$h_{TP} = (1-\alpha) h_L + \alpha h_G$$

$$= (1-\alpha) h_L \left[1 + \left(\frac{\alpha}{1-\alpha} \right) \left(\frac{h_G}{h_L} \right) \right] \tag{4}$$

There are several well-known single-phase heat transfer correlations in the literature. In this study the Sieder and Tate [35] equation was chosen as the fundamental single-phase heat transfer correlation because of its practical simplicity and proven applicability.

Based upon this correlation, the single-phase heat transfer coefficients in Eq. (4), h_L and h_G, can be modeled as functions of Reynolds number, Prandtl number, and the ratio of bulk to wall viscosities. Thus, Eq. (4) can be expressed as:

$$h_{TP} = (1-\alpha) h_L \left[1 + \frac{\alpha}{1-\alpha} \frac{\text{fctn}\left(\text{Re}, \text{Pr}, \mu_B/\mu_W\right)_G}{\text{fctn}\left(\text{Re}, \text{Pr}, \mu_B/\mu_W\right)_L} \right] \tag{5}$$

or

$$h_{TP} = (1-\alpha) h_L \left[1 + \frac{\alpha}{1-\alpha} \text{fctn} \left\{ \left(\frac{Re_G}{Re_L} \right), \times \left(\frac{Pr_G}{Pr_L} \right), \left(\frac{(\mu_B/\mu_W)_G}{(\mu_B/\mu_W)_L} \right) \right\} \right] \tag{6}$$

Substituting the definition of Reynolds number ($Re = \rho VD/\mu_B$) for the gas (Re_G) and liquid (Re_L) yields

$$\frac{h_{TP}}{(1-\alpha)\,h_L} = 1 + \frac{\alpha}{1-\alpha}\text{fctn}\left\{\left(\frac{(\rho VD)_G(\mu_B)_L}{(\rho VD)_L(\mu_B)_G}\right), \times\left(\frac{Pr_G}{Pr_L}\right), \left(\frac{(\mu_B/\mu_W)_G}{(\mu_B/\mu_W)_L}\right)\right\} \quad (7)$$

Rearranging yields

$$\frac{h_{TP}}{(1-\alpha)h_L} = 1 + \frac{\alpha}{1-\alpha}\text{fctn}\left\{\left(\frac{\rho_G}{\rho_L}\frac{V_G}{V_L}\frac{D_G}{D_L}\right), \times\left(\frac{Pr_G}{Pr_L}\right), \left(\frac{(\mu_W)_L}{(\mu_W)_G}\right)\right\} \quad (8)$$

where the assumption has been made that the bulk viscosity ratio in the Reynolds number term of Eq. (7) is exactly canceled by the last term in Eq. (7), which includes the same bulk viscosity ratio. Substituting Eq. (1) for the ratio of gas-to-liquid diameters (D_G/D_L) in Eq. (8) and based upon practical considerations assuming that the ratio of liquid-to-gas viscosities evaluated at the wall temperature $[(\mu_W)_L/(\mu_W)_G]$ is comparable to the ratio of those viscosities evaluated at the bulk temperature (μ_L/μ_G), Eq. (8) reduces to

$$\frac{h_{TP}}{(1-\alpha)h_L} = 1 + \frac{\alpha}{1-\alpha}\text{fctn}\left\{\left(\frac{\rho_G}{\rho_L}\frac{V_G}{V_L}\frac{\sqrt{\alpha}}{\sqrt{1-\alpha}}\right), \times\left(\frac{Pr_G}{Pr_L}\right), \left(\frac{\mu_L}{\mu_G}\right)\right\} \quad (9)$$

Further simplifying Eq. (9), combine Eqs. (2) and (3) for V_G (gas velocity) and V_L (liquid velocity) to get the ratio of V_G/V_L and substitute into Eq. (9) to get

$$h_{TP} = (1-\alpha)h_L\left[1 + \text{fctn}\left\{\left(\frac{x}{1-x}\right), \left(\frac{\alpha}{1-\alpha}\right), \left(\frac{Pr_G}{Pr_L}\right), \times\left(\frac{\mu_L}{\mu_G}\right)\right\}\right] \quad (10)$$

Assuming that two-phase heat transfer coefficient can be expressed using a power-law relationship on the individual parameters that appear in Eq. (10), then it can be expressed as:

$$h_{TP} = (1-\alpha)h_L\left[1 + C\left\{\left(\frac{x}{1-x}\right)^m\left(\frac{\alpha}{1-\alpha}\right)^n \times\left(\frac{Pr_G}{Pr_L}\right)^p\left(\frac{\mu_G}{\mu_L}\right)^q\right\}\right] \quad (11)$$

where C, m, n, p, and q are adjustable constants, and h_L comes from the Sieder and Tate [35] correlation for turbulent flow,

$$h_L = 0.027Re_L^{4/5}Pr_L^{1/3}\left(\frac{k_L}{D}\right)\left(\frac{\mu_B}{\mu_W}\right)_L^{0.14} \quad (12)$$

For the Reynolds number (Re_L) in Eq. (12), the following relationship is used to evaluate the in-situ Reynolds number (liquid phase) rather than the superficial Reynolds number (Re_{SL}) as commonly used in the correlations of the available literature [11]:

$$Re_L = \left(\frac{\rho VD}{\mu}\right)_L = \frac{4\dot{m}_L}{\pi\sqrt{1-\alpha}\mu_L D} \quad (13)$$

Any other well-known single-phase turbulent heat transfer correlation could have been used in place of the Sieder and Tate [35] correlation. The difference resulting from the use of a different single-phase heat transfer correlation will be absorbed during the determination of the values of the leading coefficient and exponents on the different parameters in Eq. (11).

The values of the void fraction (α) used in Eq. (11) either were taken directly from the original experimental data sets (if available) or were calculated based on the equation provided by Chisholm [37], which can be expressed as

$$\alpha = \left[1 + \left(1 - x + x\frac{\rho_L}{\rho_G}\right)^{1/2}\left(\frac{1-x}{x}\right)\left(\frac{\rho_G}{\rho_L}\right)\right]^{-1} \quad (14)$$

In the next section the proposed heat transfer correlation, Eq. (11), is tested with four extensive sets of vertical two-phase flow heat transfer data available from the literature (see Table 1).

Table 4 Results of the predictions for available two-phase heat transfer experimental data using Eq. (11), Kim et al. [36]

	Values of constant and exponents					RMS deviation	Mean deviation	Number of data	Range of parameters			
Fluids ($Re_{SL} > 4000$)	C	m	n	p	q	(%)	(%)	within ±30%	Re_{SL}	Re_{SG}	Pr_G/Pr_L	μ_G/μ_L
All 255 data points	0.27	−0.04	1.21	0.66	−0.72	12.78	2.54	245	4000 to 127,000	14 to 209,000	9.99×10^{-3} to 137×10^{-3}	3.64×10^{-3} to 23.7×10^{-3}
Air–water [12], 105 data points						12.98	3.53	98				
Air–silicone [13], 56 data points						7.77	5.25	56				
Helium–water [14], 50 data points						15.68	−1.66	48				
Freon 12–water [14], 44 data points						13.74	1.51	43				

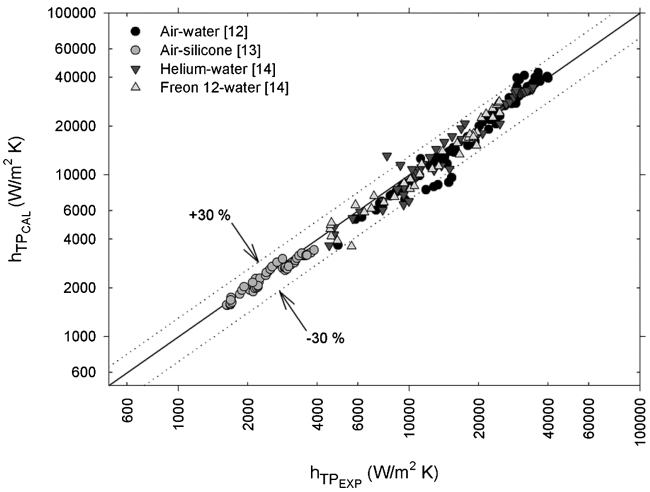

Figure 1 Comparison of the predictions by Eq. (11) with the experimental data for vertical flow (255 data points), Kim et al. [36].

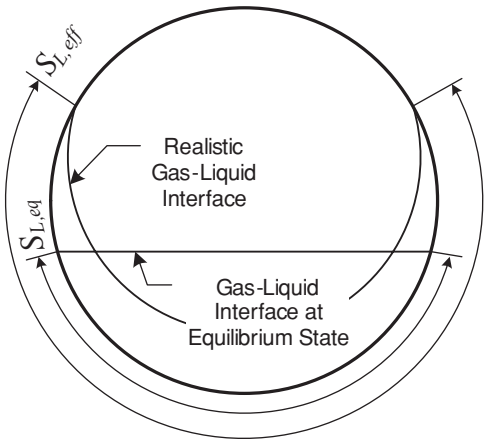

Figure 2 Gas–liquid interfaces and wetted perimeters.

HEAT TRANSFER CORRELATION FOR GAS–LIQUID FLOW IN VERTICAL PIPES

To determine the values of leading coefficient and the exponents in Eq. (11), four sets of experimental data (see the first column in Table 4) for vertical pipe flow were used. The ranges of these four sets of experimental data can be found in Kim et al. [11]. The experimental data (a total of 255 data points) included four different gas–liquid combinations (air–water, air–silicone, helium–water, Freon 12–water) and covered a wide range of variables, including liquid and gas flow rates, properties, and flow patterns.

The selected experimental data were only for turbulent two-phase heat transfer data in which the superficial Reynolds numbers of the liquid (Re_{SL}) were all greater than 4000. Table 4 and Figure 1 provide the details of the correlation and how well the proposed correlation predicted the experimental data.

The two-phase heat transfer correlation, Eq. (11), predicted the heat transfer coefficients of 255 experimental data points for vertical flow with an overall mean deviation of about 2.5% and a root-mean-square deviation of about 12.8%. About 83% of the data (212 data points) were predicted with less than ±15% deviation, and about 96% of the data (245 data points) were predicted with less than ±30% deviation. The results clearly show that the proposed heat transfer correlation is robust and can be applied to turbulent gas–liquid flow in vertical pipes with different flow patterns and fluid combinations.

A GENERAL TWO-PHASE HEAT TRANSFER CORRELATION FOR VARIOUS FLOW PATTERNS AND PIPE INCLINATIONS

The heat transfer correlation developed by Kim et al. [36], Eq. (11), was meant for predicting heat transfer rate in two-phase flow in vertical pipes. In order to handle the effects of various flow patterns and inclination angles on the two-phase heat transfer data with only one correlation, Ghajar and Kim [38] and Kim and Ghajar [39] introduced the flow pattern factor (F_P) and the inclination factor (I).

The void fraction (α), which is the volume fraction of the gas phase in the tube cross-sectional area, does not reflect the actual wetted perimeter (S_L) in the tube with respect to the corresponding flow pattern. For instance, the void fraction and the nondimensionalized wetted perimeter of annular flow both approach unity, but in the case of plug flow the void fraction is near zero and the wetted perimeter is near unity. However, the estimation of the actual wetted perimeter is very difficult due to the continuous interaction of the two phases in the tube. Therefore, instead of estimating the actual wetted perimeter, modeling the effective wetted perimeter is a more practical approach. In their model, Ghajar and his co-workers have ignored the influence of the surface tension and the contact angle of each phase on the effective wetted perimeter. The wetted perimeter at the equilibrium state, which can be calculated from the void fraction, is

$$\tilde{S}^2_{L,eq} = \left(\frac{S_{L,eq}}{\pi D}\right)^2 = 1 - \alpha \tag{15}$$

However, as shown in Figure 2, the shape of the gas–liquid interface at the equilibrium state based on the void fraction (α) is far different from the one for the realistic case. The two-phase heat transfer correlation, Eq. (11), weighted by the void fraction ($1-\alpha$), is not capable of distinguishing the differences between different flow patterns. Therefore, in order to capture the realistic shape of the gas–liquid interface, the flow pattern factor (F_P), an effective wetted-perimeter relation, which is a modified version of the equilibrium wetted perimeter, Eq. (15), is proposed:

$$F_P = \tilde{S}^2_{L,eff} = \left(\frac{S_{L,eff}}{\pi D}\right)^2 = (1-\alpha) + \alpha F_S^2 \tag{16}$$

For simplicity, the preceding equation for the effective wetted-perimeter relation ($\tilde{S}^2_{L,eff}$) is referred to as the flow pattern factor (F_P). The term (F_S) appearing in Eq. (16) is referred to as the shape factor, and in essence is a modified and normalized

Froude number. The shape factor (F_S) is defined as

$$F_S = \frac{2}{\pi}\tan^{-1}\left(\sqrt{\frac{\rho_G\,(V_G - V_L)^2}{g\,D\,(\rho_L - \rho_G)}}\right) \tag{17}$$

The shape factor (F_S) is applicable for slip ratios $K\left(= V_G/V_L\right) \geq 1$, which is common in gas–liquid flow, and represents the shape changes of the gas–liquid interface by the force acting on the interface due to the relative momentum and gravitational forces.

Due to the density difference between gas and liquid, the liquid phase is much more affected by the orientation of the pipe (inclination). A detailed discussion of the inclination effect on the two-phase heat transfer is available in Ghajar and Tang [40]. In order to account for the effect of inclination, Ghajar and Kim [38] proposed the inclination factor

$$I = 1 + \frac{g\,D\,(\rho_L - \rho_G)\,\sin\theta}{\rho_L\,V_{SL}^2} \tag{18}$$

where the term $[g\,D\,(\rho_L - \rho_G)\,\sin(\theta)]/[\rho_L\,V_{SL}^2]$ represents the relative force acting on the liquid phase in the flow direction due to the momentum and the buoyancy forces.

Now, introduce the two proposed factors for the flow pattern (F_P) and inclination (I) effects into our heat transfer correlation, Eq. (11). Substituting (F_P) for $(1-\alpha)$, which is the leading coefficient of (h_L), and introducing (I) as an additional power-law term in Eq. (11), the two-phase heat transfer correlation becomes

$$h_{TP} = F_P\,h_L\left\{1 + C\left[\left(\frac{x}{1-x}\right)^m\left(\frac{1-F_P}{F_P}\right)^n \times \left(\frac{Pr_G}{Pr_L}\right)^p\left(\frac{\mu_L}{\mu_G}\right)^q (I)^r\right]\right\} \tag{19}$$

where (h_L) comes from the Sieder and Tate [35] correlation for turbulent flow [see Eq. (12)]. For the Reynolds number needed in the (h_L) calculation, Eq. (13), presented and discussed earlier, was used. The values of the void fraction (α) used in Eqs. (13), (16), and (19) were calculated based on the correlation provided by Woldesemayat and Ghajar [41], which can be expressed as

$$\alpha = \frac{V_{SG}}{C_0\,(V_{SG} + V_{SL}) + u_{GM}} \tag{20}$$

where the distribution parameter (C_0) and the drift velocity of gas (u_{GM}) are given as

$$C_0 = \frac{V_{SG}}{V_{SG} + V_{SL}}\left[1 + \left(\frac{V_{SL}}{V_{SG}}\right)^{(\rho_G/\rho_L)^{0.1}}\right]$$

And

$$u_{GM} = 2.9(1.22 + 1.22\sin\theta)^{(P_{atm}/P_{sys})} \times \left[\frac{g D\sigma\,(1+\cos\theta)\,(\rho_L - \rho_G)}{\rho_L^2}\right]^{0.25}$$

Note that the leading constant value of 2.9 in the preceding equation for the drift flux velocity (u_{GM}) carries a unit of $m^{-0.25}$, and Eq. (20) should be used with SI units.

Other void fraction correlations could also be used in place of the Woldesemayat and Ghajar [41] correlation. Tang and Ghajar [42] showed that Eq. (19) has such robustness that it can be applied with different void fraction correlations. The difference resulting from the use of different correlations will be absorbed during the determination of the values of the constant and exponents of Eq. (19).

The two-phase heat transfer correlation, Eq. (19), was validated with a total of 763 experimental data points for different flow patterns and inclination angles [39, 42, 43]. Overall, the correlation, Eq. (19), has successfully predicted over 85% of the experimental data points to within ±30% for 0°, 2°, 5°, and 7° pipe orientations.

However, upon revisiting the two-phase heat transfer correlation, Eq. (19), along with the equations for flow pattern factor (F_P), Eq. (16), and inclination factor (I), Eq. (18), it was realized that the correlation has not accounted for the surface tension force. Since surface tension is a variable that can affect the hydrodynamics of gas–liquid two-phase flow, it is sensible to include the surface tension into the correlation. To do that, the equation for the inclination factor (I), Eq. (18), is modified. The modified inclination factor takes on the following form:

$$I^* = 1 + Eo\,|\sin\theta| \tag{21}$$

where the Eötvös number (Eo) is defined as

$$Eo = \frac{(\rho_L - \rho_G)gD^2}{\sigma} \tag{22}$$

The Eötvös number (Eo), also known as the Bond number (Bo), represents the hydrodynamic interaction of buoyancy and surface tension forces that occur in two-phase flow. With the modification of the equation for the inclination factor, two-phase heat transfer coefficients can be estimated using the general two-phase heat transfer correlation, Eq. (19), along with the flow pattern factor (F_P), Eq. (16), and modified inclination factor (I^*), Eq. (21):

$$h_{TP} = F_P\,h_L\left[1 + C\left(\frac{x}{1-x}\right)^m\left(\frac{1-F_P}{F_P}\right)^n \times \left(\frac{Pr_G}{Pr_L}\right)^p\left(\frac{\mu_L}{\mu_G}\right)^q (I^*)^r\right] \tag{23}$$

Since Eq. (23) is considered an empirical correlation, the values of the constant and exponents C, m, n, p, q, and r are obtained with the use of experimental data. The proper values of the constant and exponents are discussed in a later section.

Table 5 Summary of experimental database sources, Woldesemayat and Ghajar [41]

Source	Physical flow configuration/characteristics	Mixture considered	Measurement technique	Number of data points
Eaton [44]	Horizontal, D = 52.5 mm and 102.26 mm	Natural gas–water	Quick-closing valves	237
Beggs [45]	Horizontal, uphill, and vertical, D = 25.4 mm, and 38. 1 mm	Air–water	Quick-closing valves	291
Spedding and Nguyen [46]	Horizontal, uphill, and vertical, D = 45.5 mm	Air–water	Quick-closing valves	1383
Mukherjee [47]	Horizontal, uphill, and vertical, D = 38.1 mm	Air–kerosene	Capacitance probes	558
Minami and Brill [48]	Horizontal, D = 77.93 mm	Air–water and air–kerosene	Quick-closing valves	54 and 57
Franca and Lahey [49]	Horizontal, D = 19 mm	Air–water	Quick-closing valves	81
Abdul-Majeed [50]	Horizontal, D = 50.8 mm	Air–kerosene	Quick-closing valves	83
Sujumnong [51]	Vertical, D = 12.7 mm	Air–water	Quick-closing valves	101

COMPARISON OF VOID FRACTION CORRELATIONS FOR DIFFERENT FLOW PATTERNS AND PIPE INCLINATIONS

Due to the importance of void fraction in influencing the characteristics of two-phase flow in pipes, Woldesemayat and Ghajar [41] conducted a very extensive comparison of 68 void fraction correlations available in the open literature against 2845 experimental data points. The experimental data points were compiled from various sources with different experimental facilities [44–51]. Out of the 2845 experimental data points, 900 were for horizontal, 1542 for inclined, and 403 for vertical pipe orientations (see Table 5).

Based on the comparison with experimental data, six void fraction correlations [52–57] were recommended for acceptably predicting void fraction for horizontal, upward inclined, and vertical pipe orientations regardless of flow patterns. The percentage of data points correctly predicted for the 2845 experimental data points within three error bands for each correlation is summarized in Table 6.

Among the six void fraction correlations listed in Table 6, Dix [53] showed better performance. The correlation by Dix [53] has the following expression:

$$\alpha = \frac{V_{SG}}{C_0\left(V_{SG} + V_{SL}\right) + u_{GM}} \tag{24}$$

Table 6 Number and percentage of data points correctly predicted by the six recommended void fraction correlations and Eq. (20) for the entire experimental database summarized in Table 5, Woldesemayat and Ghajar [41]

	Number of data points within		
Correlation	±5%	±10%	±15%
Morooka et al. [52]	1065 (37.4%)	2137 (75.1%)	2427 (85.3%)
Dix [53]	1597 (56.1%)	2139 (75.2%)	2363 (83.1%)
Rouhani and Axelsson [54]	1082 (38.0%)	2059 (72.4%)	2395 (84.2%)
Hughmark [55]	1244 (43.7%)	2003 (70.4%)	2322 (81.6%)
Premoli et al. [56]	1643 (57.8%)	2084 (73.3%)	2304 (81.0%)
Filimonov et al. [57]	1369 (48.1%)	1953 (68.6%)	2294 (80.6%)
Woldesemayat and Ghajar [41], Eq. (20)	1718 (60.4%)	2234 (78.5%)	2436 (85.6%)

Note. In total, 2845 experimental data points (see Table 5) were used in this comparison.

where the distribution parameter (C_0) and the drift velocity of gas (u_{GM}) are given as

$$C_0 = \frac{V_{SG}}{V_{SG} + V_{SL}}\left[1 + \left(\frac{V_{SL}}{V_{SG}}\right)^{\left(\rho_G/\rho_L\right)^{0.1}}\right]$$

And

$$u_{GM} = 2.9\left[\frac{g\sigma\left(\rho_L - \rho_G\right)}{\rho_L^2}\right]^{0.25}$$

Figure 3 shows the performance of the void fraction correlation by Dix [53], Eq. (24). Woldesemayat and Ghajar [41] proposed an improved void fraction correlation, Eq. (20), that gives better predictions when compared with available experimental data. The performance of Eq. (20) on the 2845 experimental data points in comparison with the recommended six void fraction correlations is also summarized in Table 6.

As shown in Table 6, the void fraction correlation, Eq. (20), introduced by Woldesemayat and Ghajar [41] gives noticeable improvements over the other six correlations. The results of the comparison for Eq. (20) with the 2845 experimental data points are also illustrated in Figure 4. Both Table 6 and Figure 4 show

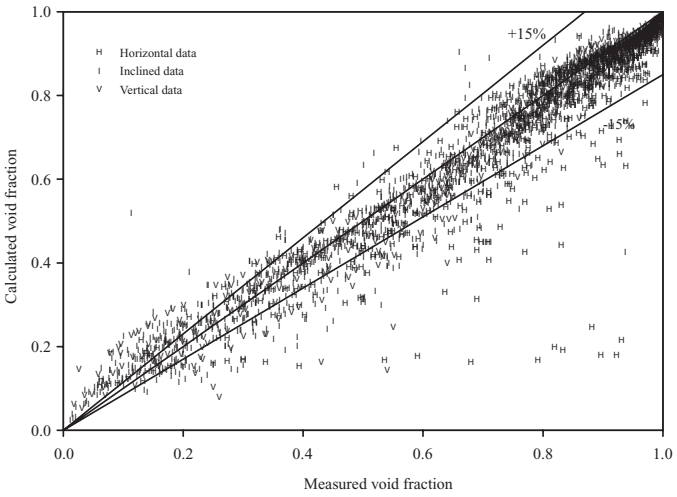

Figure 3 Comparison of void fraction correlation by Dix [53], Eq. (24), with 2845 experimental data points summarized in Table 5, Woldesemayat and Ghajar [41].

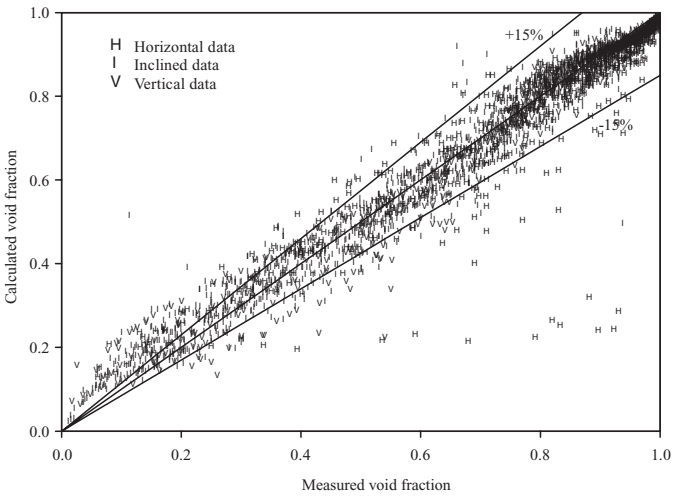

Figure 4 Comparison of void fraction correlation by Woldesemayat and Ghajar [41], Eq. (20), with 2845 experimental data points summarized in Table 5, Woldesemayat and Ghajar [41].

the capability and robustness of Eq. (20) to successfully predict void fraction for various pipe sizes, inclinations, and two-phase fluid mixtures from various sources with different experimental facilities. The benefit of comparing with experimental data from different facilities is the minimization of sample bias.

EXPERIMENTAL SETUP AND DATA REDUCTION FOR HORIZONTAL AND SLIGHTLY UPWARD INCLINED PIPE FLOW

A schematic diagram of the overall experimental setup for heat transfer measurements is shown in Figure 5. The test section is a 27.9 mm inner diameter (I.D.) straight standard stainless steel schedule 10S pipe with a length to diameter ratio of 95. The setup rests atop a 9 m long aluminum I-beam that is supported by a pivoting foot and a stationary foot that incorporates a small electric screw jack.

In order to apply uniform wall heat flux boundary condition to the test section, copper plates were silver soldered to the inlet and exit of the test section. The uniform wall heat flux boundary condition was maintained by a Lincoln SA-750 welder for $Re_{SL} > 2000$ and a Miller Maxtron 450 DC welder for $Re_{SL} < 2000$. The entire length of the test section was wrapped using fiberglass pipe wrap insulation, followed by a thin polymer vapor seal to prevent moisture penetration. The calming section (clear polycarbonate pipe with 25.4 mm I.D. and L/D = 88) served as a flow developing and turbulence reduction device and flow pattern observation section.

T-type thermocouple wires were cemented with Omegabond 101, an epoxy adhesive with high thermal conductivity and electrical resistivity, on the outside wall of the stainless steel test section as shown in Figure 6. Thermocouples were placed on the outer surface of the pipe wall at uniform intervals of 254 mm from the entrance to the exit of the test section. There were 10 thermocouple stations in the test section (refer to Figure 6). All the thermocouples were monitored with a National Instruments data acquisition system. The average system stabilization time period was from 30 to 60 min after the system attained steady state. The inlet liquid and gas temperatures and the exit bulk temperature were measured by Omega TMQSS-125U-6 thermocouple probes. Calibration of thermocouples and thermocouple probes showed that they were accurate to within $\pm 0.5^{\circ}$C. The operating pressures inside the experimental setup were monitored with a pressure transducer. To ensure a uniform fluid bulk temperature at the inlet and exit of the test section, a mixing well of alternating polypropylene baffle type static mixer for both gas and liquid phases was utilized. The outlet bulk temperature was measured immediately after the mixing well.

The fluids used in the test loop are air and water. The water is distilled and stored in a 55-gal cylindrical polyethylene tank. A Bell & Gosset series 1535 coupled centrifugal pump was used to pump the water through an Aqua-Pure AP12T water filter. An ITT Standard model BCF 4063 one-shell and two-tube pass heat exchanger removes the pump heat and the heat added during the test to maintain a constant inlet water temperature. From the heat exchanger, the water passes through a Micro Motion Coriolis flow meter (model CMF100) connected to a digital Field-Mount Transmitter (model RFT9739) that conditions the flow information for the data acquisition system. From the Coriolis flow meter it then flows into the test section. Air is supplied via an Ingersoll-Rand T30 (model 2545) industrial air compressor. The air passes through a copper coil submerged in a vessel of water to lower the temperature of the air to room temperature. The air is then filtered and condensation is removed in a coalescing filter. The air flow is measured by a Micro Motion Coriolis flow meter (model CMF025) connected to a digital Field-Mount Transmitter (model RFT9739) and regulated by a needle valve. Air is delivered to the test section by flexible tubing. The water and air mixture is returned to the reservoir, where it is separated and the water is recycled.

The heat transfer measurements at uniform wall heat flux boundary condition were carried out by measuring the local outside wall temperatures at 10 stations along the axis of the pipe and the inlet and outlet bulk temperatures, in addition to other measurements such as the flow rates of gas and liquid, room temperature, voltage drop across the test section, and current carried by the test section. A National Instruments data acquisition system was used to record and store the data measured during these experiments. The computer interface used to record the data is a LabVIEW Virtual Instrument (VI) program written for this specific application.

The peripheral heat transfer coefficient (local average) was calculated based on the knowledge of the pipe inside wall surface temperature and inside wall heat flux obtained from a data reduction program developed exclusively for this type of experiment [58]. The local average peripheral values for inside wall temperature, inside wall heat flux, and heat transfer coefficient were then obtained by averaging all the appropriate individual

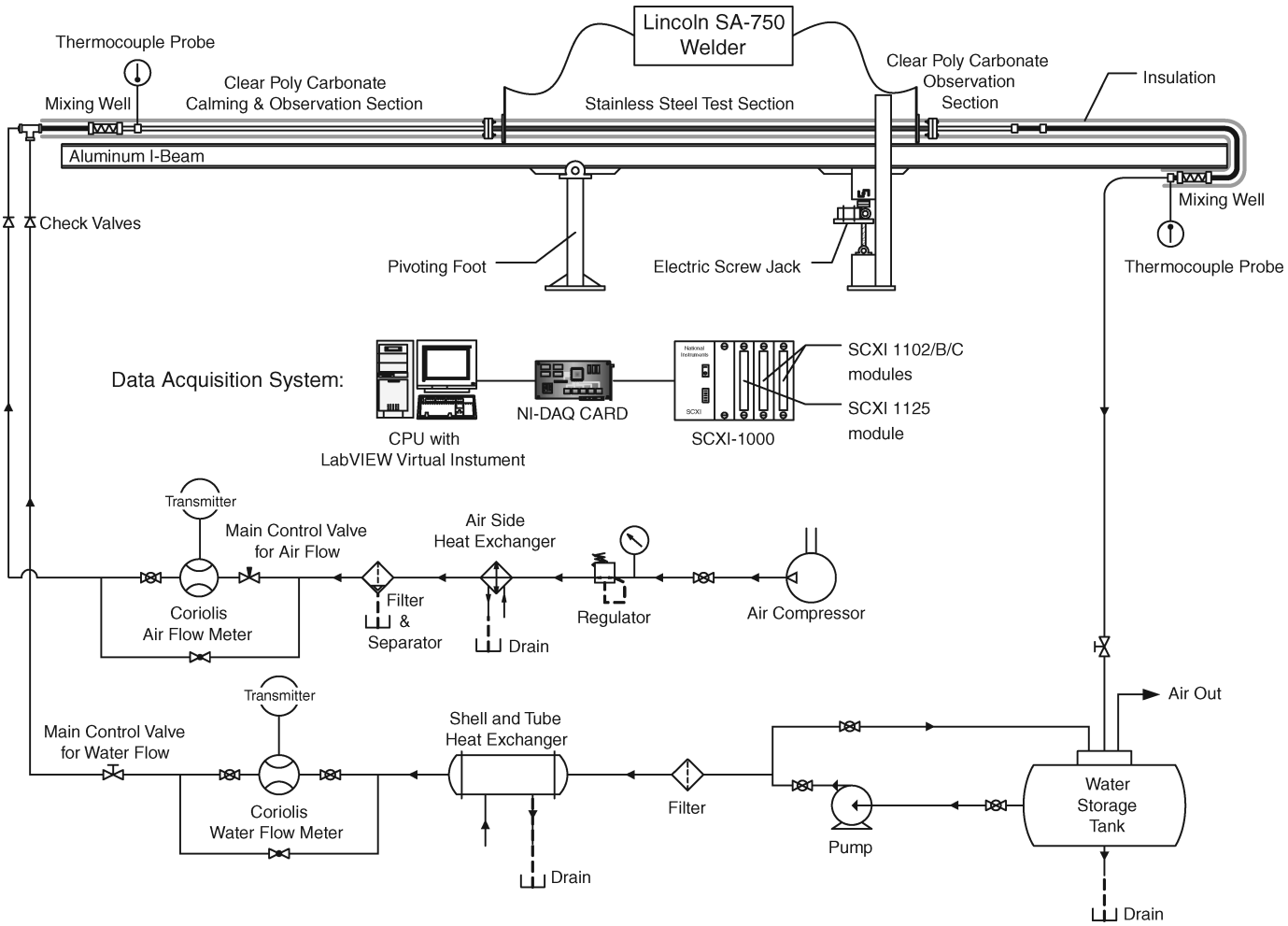

Figure 5 Schematic of experimental setup.

local peripheral values at each axial location. The variation in the circumferential wall temperature distribution, which is typical for two-phase gas–liquid flow in horizontal pipes, leads to different heat transfer coefficients depending on which circumferential wall temperature is selected for the calculations. In two-phase heat transfer experiments, in order to overcome the unbalanced circumferential heat transfer coefficients and to get a representative heat transfer coefficient for a test run, the following equation was used to calculate an overall two-phase heat transfer coefficient ($h_{TP_{EXP}}$) for each test run:

$$h_{TP_{EXP}} = \frac{1}{L}\int \bar{h}\, dz = \frac{1}{L}\sum_{k=1}^{N_{ST}} \bar{h}_k\, \Delta z_k$$

$$= \frac{1}{L}\sum_{k=1}^{N_{ST}} \left(\frac{\bar{q}''}{\bar{T}_w - T_B}\right)_k \Delta z_k \qquad (25)$$

where L is the length of the test section, and $\bar{h}$, $\bar{q}''$, $\bar{T}_w$, and T_B are the local mean heat transfer coefficient, the local mean heat flux, the local mean wall temperature, and the bulk temperature at a thermocouple station, respectively; k is the index of the thermocouple stations, N_{ST} is the number of the thermocouple stations, z is the axial coordinate, and Δz is the element length of each thermocouple station. The data reduction program used a finite-difference formulation to determine the inside wall temperature and the inside wall heat flux from measurements of the outside wall temperature, the heat generation within the pipe wall, and the thermophysical properties of the pipe material (electrical resistivity and thermal conductivity).

The reliability of the flow circulation system and of the experimental procedures was checked by making several single-phase calibration runs with distilled water. The single-phase heat transfer experimental data were checked against the well-established single-phase heat transfer correlations [59] in the Reynolds number range from 3000 to 30,000. In most instances, the majority of the experimental results were well within ±10% of the predicted results [59, 60].

The uncertainty analysis of the overall experimental procedures using the method of Kline and McClintock [61] showed that there is a maximum of 11.5% uncertainty for heat transfer coefficient calculations. Experiments under the same conditions

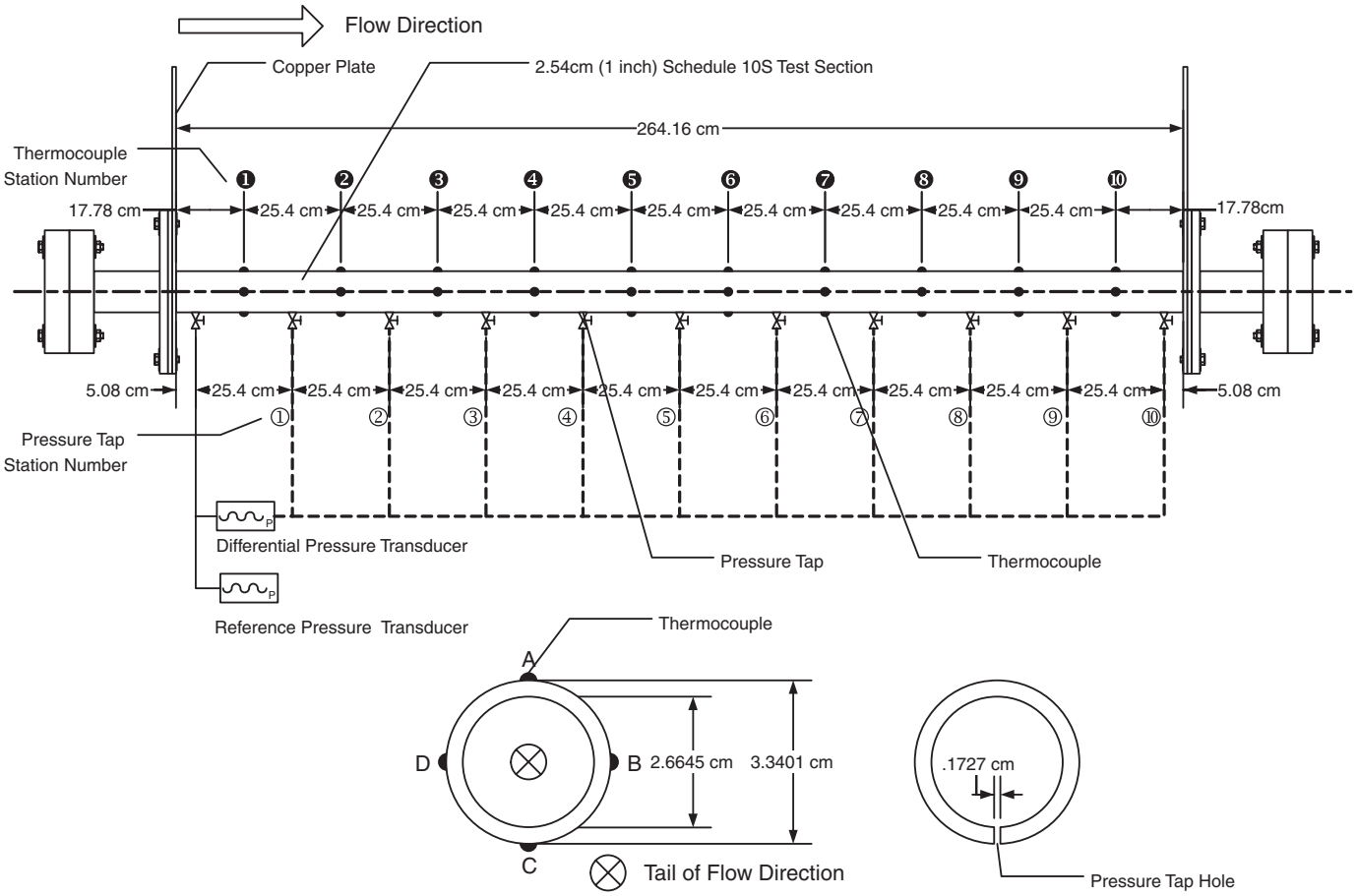

Figure 6 Test section.

were conducted periodically to ensure the repeatability of the results. The maximum difference between the duplicated experimental runs was within ±10%.

FLOW PATTERNS

The various interpretations accorded to the multitude of flow patterns by different investigators are subjective; no uniform procedure exists at present for describing and classifying them. In this study, the flow pattern identification for the experimental data was based on the procedures suggested by Taitel and Dukler [62] and by Kim and Ghajar [59], and on visual observations as deemed appropriate. All observations for the flow pattern judgments were made at the clear polycarbonate observation sections before and after the stainless steel test section (see Figure 5). By fixing the water flow rate, flow patterns were observed by varying air flow rates.

Flow pattern data were obtained at isothermal condition with the pipe in horizontal position and at 2°, 5°, and 7° inclined positions. These experimental data were plotted and compared using their corresponding values of Re_{SG} and Re_{SL} and the flow patterns. Representative digital images of each flow pattern were taken using a Nikon D50 digital camera with Nikkor 50 mm f/1.8D lens. Figure 7 shows the flow map for horizontal flow with the representative photographs of the various flow patterns. The various flow patterns for horizontal flow depicted in Figure 7 show the capability of our experimental setup to cover a multitude of flow patterns. The shaded regions represent the transition boundaries of the observed flow patterns.

The influence of small inclination angles of 2°, 5°, and 7° on the observed flow patterns is shown in Figure 8. As shown in this

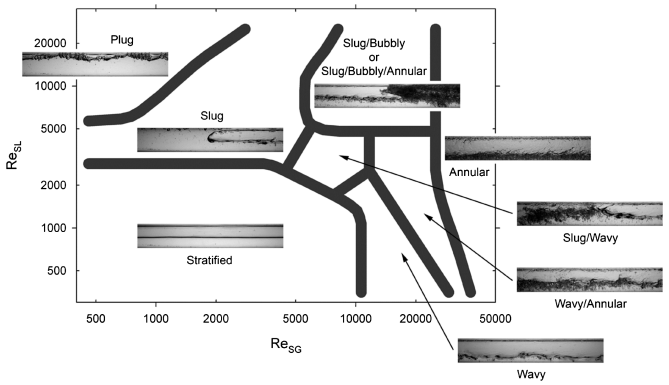

Figure 7 Flow map for horizontal flow with representative photographs of flow patterns.

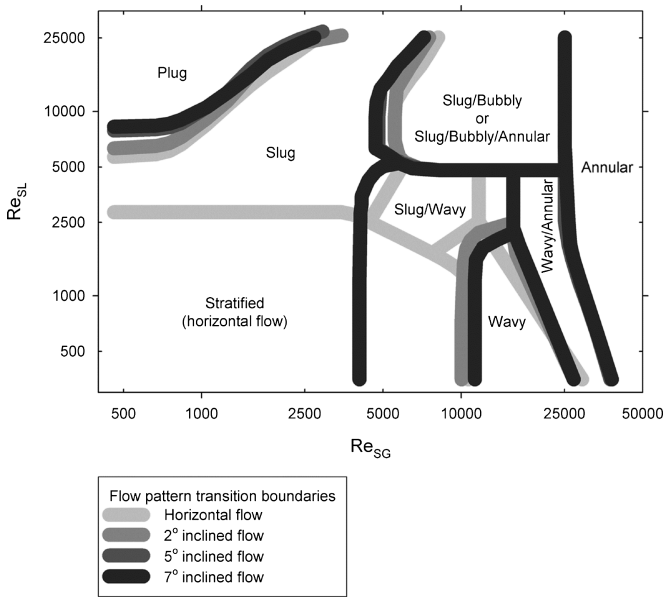

Figure 8 Change of flow pattern transition boundaries as pipe inclined upward from horizontal position.

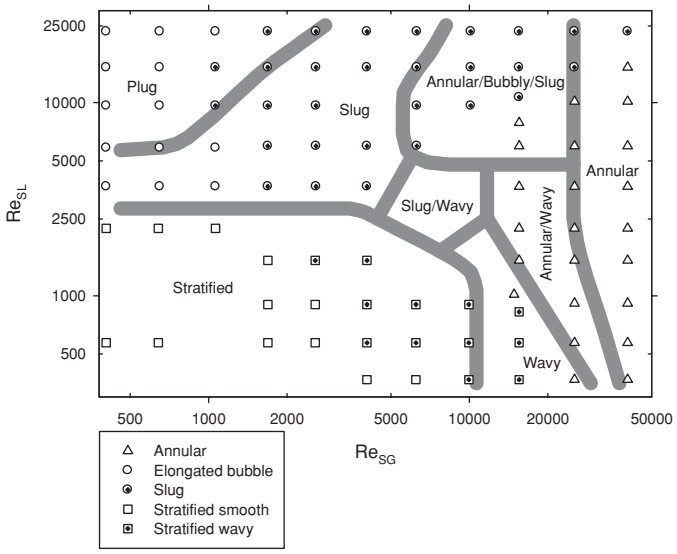

Figure 9 Flow patterns data points from Barnea et al. [63] plotted on the flow map for horizontal flow (see Figure 7).

figure, the flow pattern transition boundaries for horizontal flow were found to be quite different from the flow pattern transition boundaries for inclined flow when slight inclinations of 2°, 5°, and 7° were introduced. The changes in the flow pattern transition boundaries from horizontal to slightly inclined flow are the transition boundaries for stratified flow and slug/wavy flow. When the pipe was inclined from horizontal to slight inclination angles of 2°, 5°, and 7°, the stratified flow region was replaced by slug flow and slug/wavy flow for $Re_{SG} < 4000$ and $4000 < Re_{SG} < 10000$, respectively.

Other shifts in the flow pattern transition boundaries were observed in the plug-to-slug boundary and the slug-to-slug/bubbly boundary. In these two cases, the flow pattern transition boundaries were observed to be shifted slightly to the upper left direction as inclination angles were slightly increased from horizontal to 7°. For slightly inclined flow of 2°, 5°, and 7°, there were no drastic changes in the flow pattern transition boundaries.

For verification of the flow pattern map, flow patterns data from Barnea et al. [63] were used and compared with the flow pattern maps for horizontal and 2° inclined pipe. Using flow pattern data from Barnea et al. [63] for air–water flow in 25.5 mm horizontal pipe, the data points plotted on the flow map for horizontal flow (see Figure 7) are illustrated in Figure 9.

The comparison between the data points from Barnea et al. [63] and the flow pattern map for horizontal flow showed very satisfactory agreement, especially among the distinctive major flow patterns such as annular, slug, and stratified. It should be noted that Barnea et al. [63] had successfully compared their horizontal flow pattern data with the flow map proposed by Mandhane et al. [64].

In a similar manner, using flow pattern data from Barnea et al. [63] for air–water flow in 25.5 mm 2° inclined pipe, the data points plotted on the flow map for 2° inclined flow (see Figure 8) are illustrated in Figure 10. The comparison between the data points from Barnea et al. [63] and the flow pattern map for 2° inclined flow also showed very satisfactory agreement.

Although the flow patterns may have similar names for both horizontal and inclined flow, this does not mean that the flow patterns in the inclined positions have identical characteristics of the comparable flow patterns in the horizontal position. For example, it was observed that the slug flow patterns in the inclined positions of 5° and 7° have reverse flow between slugs due to the gravitational force, which can have a significant effect on the heat transfer. To understand the influence of flow patterns on heat transfer, systematic measurement of heat transfer data were conducted. Table 7 and Figure 11 illustrate the number of two-phase heat transfer data points systematically measured for different flow patterns and test section orientations. Heat

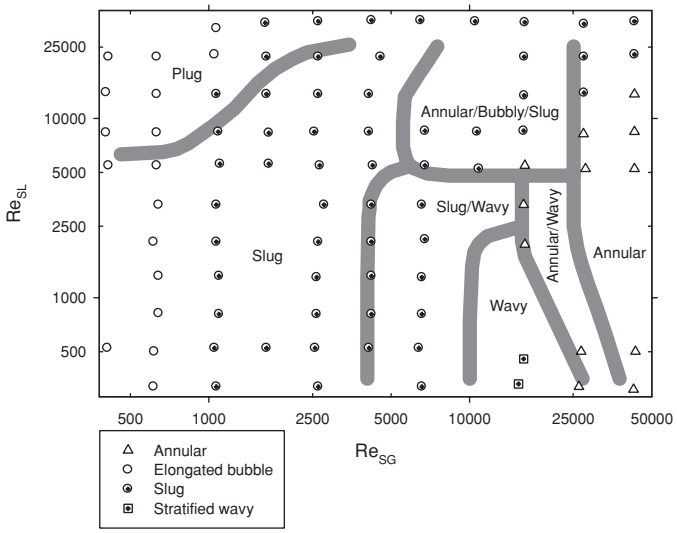

Figure 10 Flow patterns data points from Barnea et al. [63] plotted on the flow map for 2° inclined flow (see Figure 8).

Table 7 Number of two-phase heat transfer data points measured for different flow patterns and pipe orientations

	Test section orientation			
Flow patterns	Horizontal	2° inclined	5° inclined	7° inclined
Stratified	20			
Slug	39	44	43	40
Plug	13	14	11	12
Slug/wavy	7	15	15	15
Wavy	10	8	10	10
Wavy/annular	22	11	9	9
Slug/bubbly/annular	40	47	50	52
Annular	57	45	46	49

transfer data at low air and water flow rates ($Re_{SG} < 500$ and $Re_{SL} < 700$) were not collected. At such low air and water flow rates, there exists the possibility of local boiling or dry-out, which could potentially damage the heated test section.

SYSTEMATIC INVESTIGATION ON TWO-PHASE GAS–LIQUID HEAT TRANSFER IN HORIZONTAL AND SLIGHTLY UPWARD INCLINED PIPE FLOWS

In this section, an overview of the different trends that have been observed in the heat transfer behavior of the two-phase air–water flow in horizontal and inclined pipes for various flow patterns is presented. The non-boiling two-phase heat transfer data were obtained by systematically varying the air and water flow rates and the pipe inclination angle. The summary of the experimental conditions and measured heat transfer coefficients are tabulated in Table 8. Detailed discussions on the complete experimental results are documented by Ghajar and Tang [40].

Figures 12 and 13 provide an overview of the pronounced influence of the flow pattern, superficial liquid Reynolds number (water flow rate) and superficial gas Reynolds number (air flow rate) on the two-phase heat transfer coefficient in horizontal flow. The results presented in Figure 12 clearly show that two-phase heat transfer coefficient is strongly influenced by the superficial liquid Reynolds number (Re_{SL}).

As shown in Figure 12, the heat transfer coefficient increases proportionally as Re_{SL} increases. In addition, for a fixed Re_{SL}, the two-phase heat transfer coefficient is also influenced by the superficial gas Reynolds number (Re_{SG}), and each flow pattern shows its own distinguished heat transfer trend, as shown in Figure 13. Typically, heat transfer increases at low Re_{SG} (the regime of plug flow), and then slightly decreases at the mid range of Re_{SG} (the regime of slug and slug-type transitional flows), and increases again at the high Re_{SG} (the regime of annular flow).

Table 8 Summary of experimental conditions and measured two-phase heat transfer data

	Test section orientation			
Parameter	Horizontal	2° inclined	5° inclined	7° inclined
Number of data points	208	184	184	187
Re_{SL} range	740–26,100	750–25,900	780–25,900	770–26,000
Re_{SG} range	700–47,600	700–47,500	590–47,500	560–47,200
Heat flux range [W/m^2]	1860–10,800	2820–10,800	2900–10,800	2600–10,900
h_{TPEXP} range [W/m^2-K]	101–5457	242–5140	286–5507	364–5701

COMPARISON OF GENERAL HEAT TRANSFER CORRELATION WITH EXPERIMENTAL RESULTS FOR VARIOUS FLOW PATTERNS AND PIPE INCLINATIONS

The two-phase heat transfer correlation, Eq. (19), was validated with a total of 763 experimental data points for different flow patterns in horizontal and slightly inclined air–water two-phase pipe flows [39, 42, 43]. Equation (19) performed relatively well by predicting over 85% of the experimental data points to within ±30% for 0°, 2°, 5°, and 7° pipe orientations. Recently, Franca et al. [65] compared their mechanistic model developed for convective heat transfer in gas–liquid intermittent (slug) flows with the general heat transfer correlation proposed in this study. For void fraction, Franca et al. [65] used their own experimental data, which were obtained for air–water flow in a 15 m long, 25.4 mm inside diameter copper pipe. When comparing their mechanistic model with Eq. (19), the agreement is within ±15%, which is considered to be excellent.

However, when comparing the heat transfer correlation, Eq. (19), with data from vertical pipes and different gas–liquid combinations, Eq. (19) has shown some inadequacy in its performance. Equation (19) was validated with 986 experimental data points for different flow patterns, inclination angles, and gas–liquid combinations. The 986 experimental data points were compiled from various sources with different experimental facilities (see Table 9) with a wide range of superficial gas and liquid Reynolds numbers ($750 \leq Re_{SL} \leq 127{,}000$ and $14 \leq Re_{SG} \leq 209{,}000$) and inclination angles ($0° \leq \theta \leq 90°$). Figure 14 shows the comparison of Eq. (19) with all 986 experimental data points for different inclination angles and gas–liquid combinations.

Figure 14 shows that Eq. (19) performed well for two-phase flow with heat transfer coefficient between 1000 W/m^2-K and 5000 W/m^2-K. However, Eq. (19) has shown some inadequacy in predicting two-phase flow with heat transfer coefficients below 1000 W/m^2-K and above 5000 W/m^2-K. Overall, Eq. (19) successfully predicted 83% of the 986 experimental data points within ±30% agreement (see Table 9). The results shown in Table 9 and Figure 14 prompted further investigation and improvements were made on Eq. (19).

As discussed previously, improvements on Eq. (19) were made by modifying the inclination factor (I), Eq. (18). The modified inclination factor (I*), Eq. (21), which includes the Eötvös number (Eo) to represent the hydrodynamic interaction

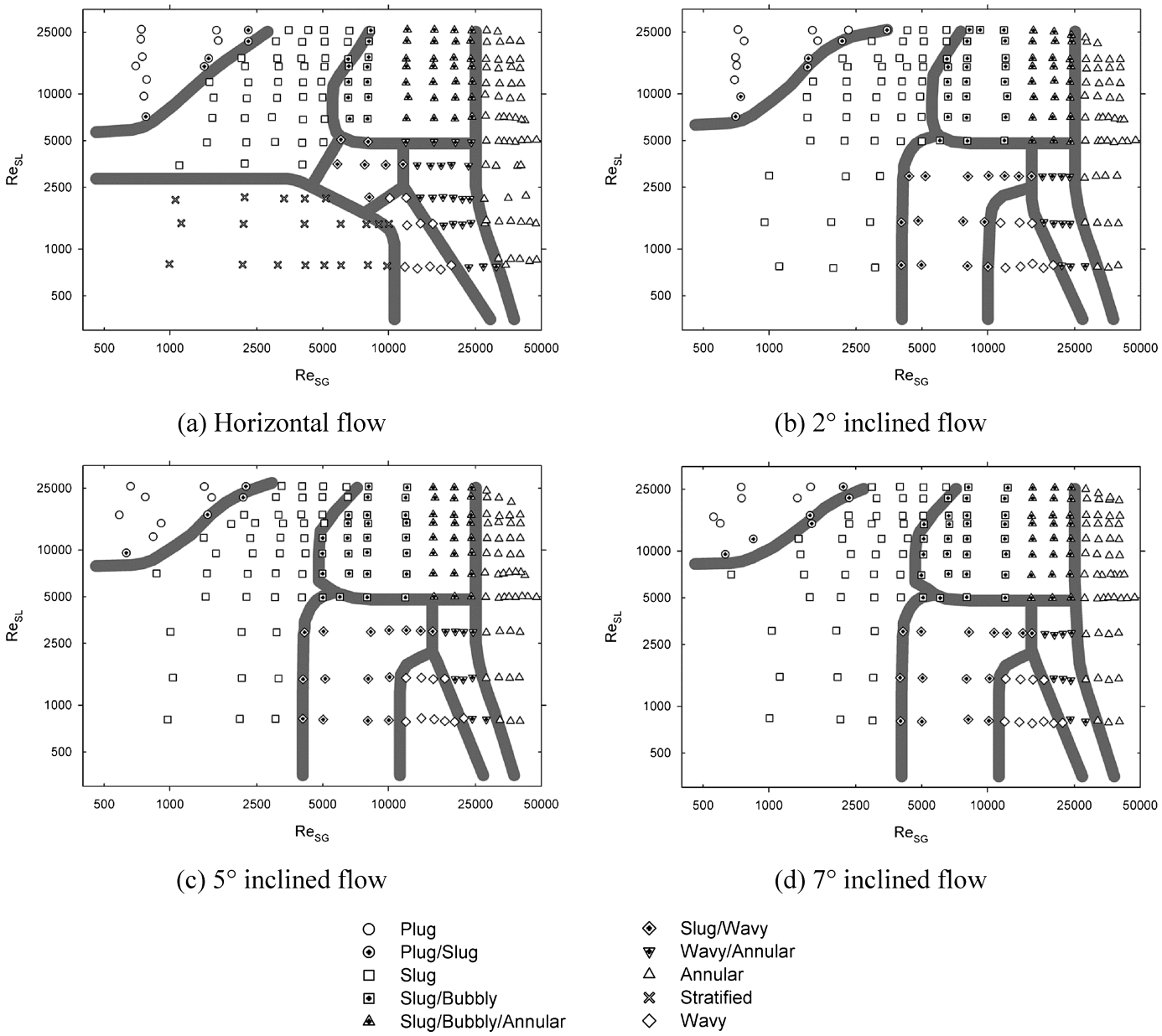

Figure 11 Flow maps for horizontal, 2°, 5°, and 7° inclined flows with distribution of heat transfer data collected.

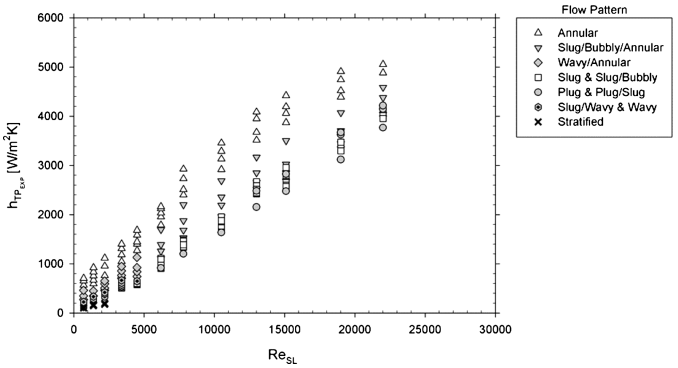

Figure 12 Variation of two-phase heat transfer coefficient with superficial liquid Reynolds number in horizontal flow.

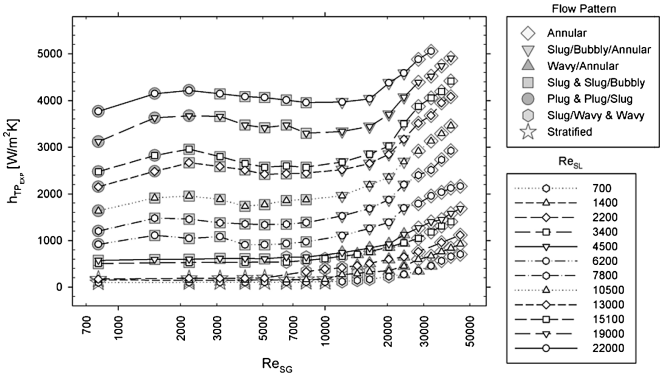

Figure 13 Variation of two-phase heat transfer coefficient with superficial gas Reynolds number in horizontal flow.

Table 9 Results of the predictions for 986 experimental heat transfer data points with different gas–liquid combinations and inclination angles by using Eq. (19)

Data set	RMS deviation (%)	Number of data points within ±20%	Number of data points within ±25%	Number of data points within ±30%	Average deviation range (%)	Range of parameters			
						Re_{SL}	Re_{SG}	Pr_G/Pr_L	μ_G/μ_L
All 986 data points, $0^\circ \le \theta \le 90^\circ$	33.1	649 (66%)	746 (76%)	817 (83%)	−16.9 to 30.8	750 to 127,000	14 to 209,000	9.99×10^{-3} to 148×10^{-3}	3.64×10^{-3} to 26.3×10^{-3}
Air–water ($\theta = 0^\circ$), 160 data points [40], 16 data points [65]	20.5	111 (63%)	140 (80%)	154 (88%)	−12.6 to 18.6	2100 to 67,000	700 to 48,000		
Air–water ($\theta = 2^\circ$), 184 data points [40]	24.9	143 (78%)	154 (84%)	168 (91%)	−12.7 to 23.0	750 to 26,000	700 to 48,000		
Air–water ($\theta = 5^\circ$), 184 data points [40]	43.4	124 (67%)	137 (74%)	150 (82%)	−15.9 to 64.5	780 to 26,000	600 to 48,000		
Air–water ($\theta = 7^\circ$), 187 data points [40]	44.7	110 (59%)	132 (71%)	149 (80%)	−16.3 to 74.7	770 to 26,000	560 to 47,000		
Air–water ($\theta = 90^\circ$), 105 data points [12]	25.0	67 (64%)	79 (75%)	85 (81%)	−22.3 to 2.4	4000 to 127,000	43 to 154,000		
Air–silicone ($\theta = 90^\circ$), 56 data points [13]	5.9	56 (100%)	56 (100%)	56 (100%)	−4.6 to 6.1	8400 to 21,000	52 to 42,000		
Helium–water ($\theta = 90^\circ$), 50 data points [14]	25.4	22 (44%)	31 (62%)	37 (74%)	−25.9 to 6.9	4000 to 126,000	14 to 13,000		
Freon 12–water ($\theta = 90^\circ$), 44 data points [14]	39.1	16 (36%)	17 (39%)	18 (41%)	−33.3 to 0	4200 to 55,000	860 to 209,000		

Note. Values of constant and exponents: C = 0.82, m = 0.08, n = 0.39, p = 0.03, q = 0.01, and r = 0.40.

of buoyancy and surface tension forces, replaced the inclination factor (I) and resulted in a generalized two-phase heat transfer correlation for various pipe inclinations and gas–liquid combinations, Eq. (23).

With the proposed constant and exponents, C = 0.55, m = 0.1, n = 0.4, and p = q = r = 0.25, Eq. (23) was successfully validated with a total of 986 experimental data points for different flow patterns, inclination angles, and gas–liquid combinations. The 986 experimental data points were compiled from various sources with different experimental facilities (see Table 10) with a wide range of superficial gas and liquid Reynolds numbers ($750 \le Re_{SL} \le 127{,}000$ and $14 \le Re_{SG} \le 209{,}000$) and inclination angles ($0^\circ \le \theta \le 90^\circ$).

As summarized in Table 10, the comparison of the predictions by the general two-phase heat transfer correlation, Eq. (23), confirmed that the correlation is adequately robust. Of all the 986 experimental data points, Eq. (23) has successfully predicted 90% of the data points within ±25% agreement with the experimental results. Overall, the prediction by Eq. (23) has a root-mean-square deviation of 18.4% from the experimental data.

Figure 15 shows the comparison of the calculated h_{TP} values from the general heat transfer correlation, Eq. (23), with all 986

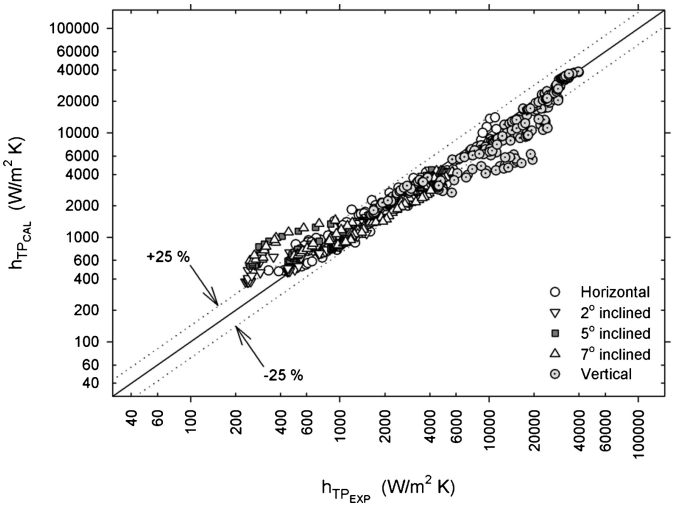

Figure 14 Comparison of the predictions by Eq. (19) with all 986 experimental data points for different inclination angles and gas–liquid combinations (see Table 9).

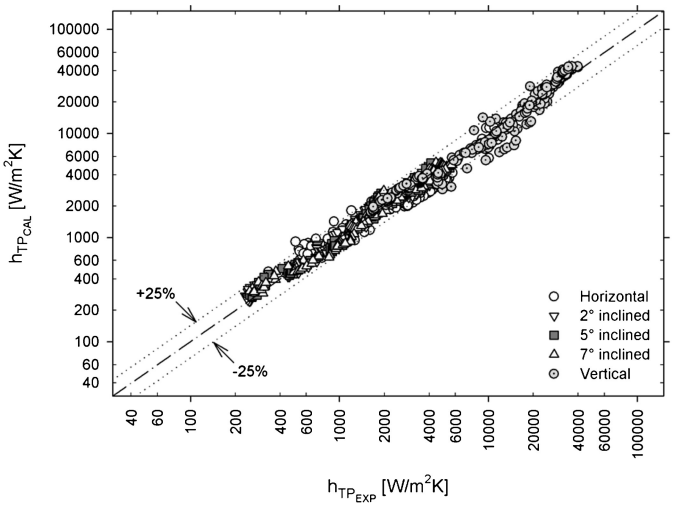

Figure 15 Comparison of the predictions by Eq. (23) with all 986 experimental data points for different inclination angles and gas–liquid combinations (see Table 10).

Table 10 Results of the predictions for 986 experimental heat transfer data points with different gas–liquid combinations and inclination angles by using Eq. (23)

Data set	RMS deviation (%)	Number of data points within ±20%	Number of data points within ±25%	Number of data points within ±30%	Average deviation range (%)	Range of parameters			
						Re_{SL}	Re_{SG}	Pr_G/Pr_L	μ_G/μ_L
All 986 data points, $0^\circ \le \theta \le 90^\circ$	18.4	793 (80%)	884 (90%)	922 (94%)	−15.3 to 12.5	750 to 127,000	14 to 209,000	9.99×10^{-3} to 148×10^{-3}	3.64×10^{-3} to 26.3×10^{-3}
Air–water ($\theta = 0^\circ$), 160 data points [40], 16 data points [65]	22.2	127 (72%)	152 (86%)	164 (93%)	−16.2 to 20.4	2100 to 67,000	700 to 48,000		
Air–water ($\theta = 2^\circ$), 184 data points [40]	13.0	161 (88%)	178 (97%)	184 (100%)	−9.2 to 12.9	750 to 26,000	700 to 48,000		
Air–water ($\theta = 5^\circ$), 184 data points [40]	12.1	154 (84%)	169 (92%)	174 (95%)	−7.7 to 11.8	780 to 26,000	600 to 48,000		
Air–water ($\theta = 7^\circ$), 187 data points [40]	12.3	164 (88%)	174 (93%)	176 (94%)	−10.3 to 9.5	770 to 26,000	560 to 47,000		
Air–water ($\theta = 90^\circ$), 105 data points [12]	23.8	79 (75%)	92 (88%)	95 (90%)	−24.5 to 11.4	4000 to 127,000	43 to 154,000		
Air–silicone ($\theta = 90^\circ$), 56 data points [13]	10.3	37 (66%)	42 (75%)	47 (84%)	−1.7 to 9.4	8400 to 21,000	52 to 42,000		
Helium–water ($\theta = 90^\circ$), 50 data points [14]	28.3	41 (82%)	42 (84%)	46 (92%)	−25.9 to 17.6	4000 to 126,000	14 to 13,000		
Freon 12–water ($\theta = 90^\circ$), 44 data points [14]	29.8	30 (68%)	35 (80%)	36 (82%)	−24.9 to 4.0	4200 to 55,000	860 to 209,000		

Note. Values of constant and exponents: C = 0.55, m = 0.1, n = 0.4, and p = q = r = 0.25.

experimental data points for different inclination angles and gas–liquid combinations. The comparison of the predictions by Eq. (23) with experimental data for air–water horizontal flow is shown in Figure 16. The results illustrated in Figure 16 show that the introduction of the flow pattern factor, Eq. (16), into the general heat transfer correlation, Eq. (23), provides the needed capability to handle different flow patterns.

Figure 17 shows the comparison of the predictions by Eq. (23) with experimental data for air–water in slightly inclined pipes (2°, 5°, and 7°). Finally, as illustrated in Figure 18, the comparison of the predictions by Eq. (23) with experimental data for various gas–liquid combinations in vertical pipes shows that the modified inclination factor (I^*)—see Eq. (21)—has adequately accounted for the inclination effects.

PRACTICAL ILLUSTRATIONS OF USING THE GENERAL TWO-PHASE HEAT TRANSFER CORRELATION

The general two-phase heat transfer correlation, Eq. (23), is applicable for estimating heat transfer coefficients for nonboiling two-phase, two-component (liquid and permanent gas)

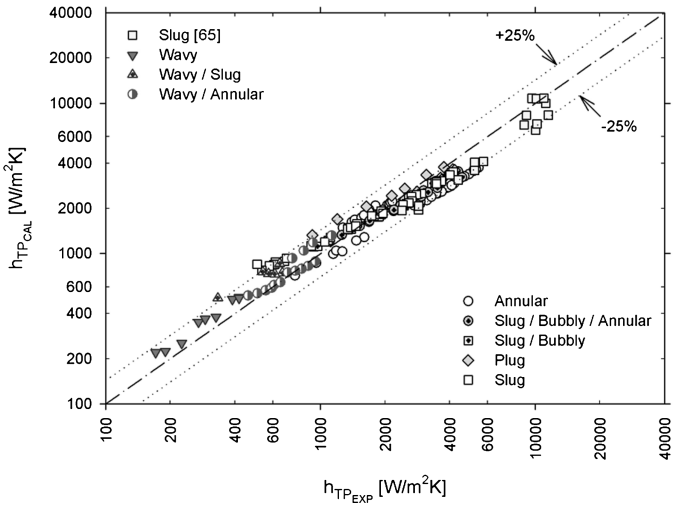

Figure 16 Comparison of the predictions by Eq. (23) with experimental data for air–water horizontal pipe flow (see Table 10).

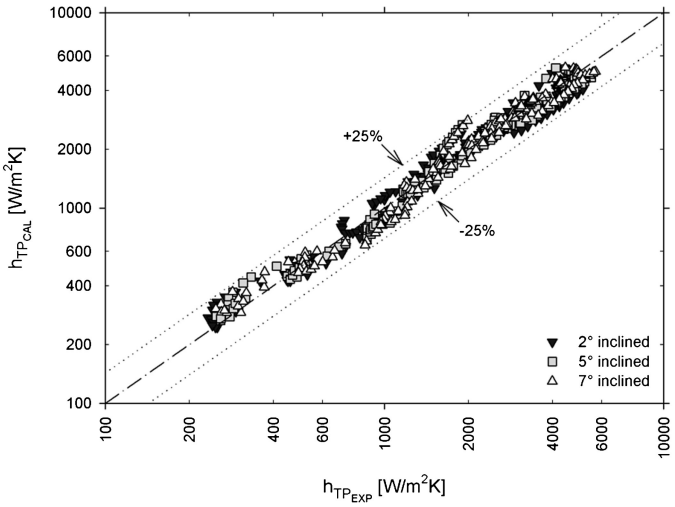

Figure 17 Comparison of the predictions by Eq. (23) with experimental data for air–water in slightly inclined pipes (see Table 10).

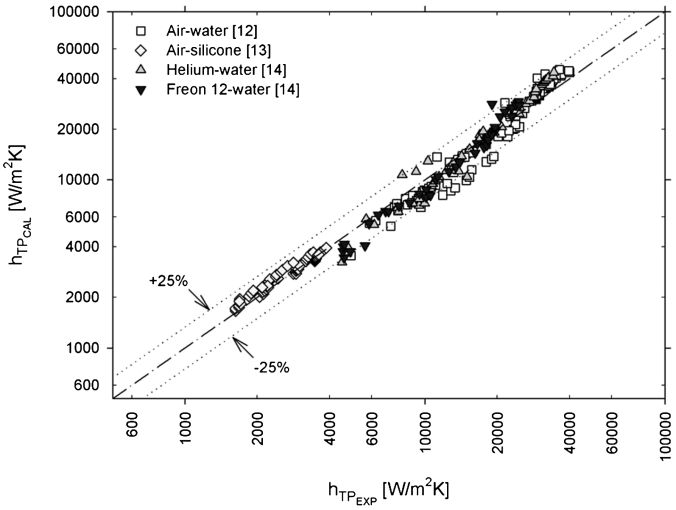

Figure 18 Comparison of the predictions by Eq. (23) with experimental data for various gas–liquid combinations in vertical pipes (see Table 10).

flow in pipes. In this section, three illustrations of using the general two-phase heat transfer correlation, Eq. (23), are discussed. The first illustration is about the application of the correlation on air and gas–oil flow in a vertical pipe with gas-to-liquid volume ratio of approximately two. The second illustration is with air and silicone (Dow Corning 200 Fluid, 5 cs) in a vertical pipe with liquid-to-gas volume ratio of approximately 90. Finally, the third illustration is an application of the correlation on air and water pipe flow in microgravity condition.

Application in Air and Gas–Oil Flow

Dorresteijn [22] conducted an experimental study of heat transfer in non-boiling two-phase flow of air and gas–oil through a 70 mm diameter vertical tube. The liquid phase consists of domestic grade gas–oil with kinematic viscosity (ν_L) of 4.7×10^{-6} m^2/s and Prandtl number (Pr_L) of approximately 60 [22]. In the conditions at which $V_{SG} = 8$ m/s, $V_{SL} = 3.16$ m/s, $\rho_G = 2.5$ kg/m^3, $\rho_L = 835$ kg/m^3, and $\alpha = 0.67$, Dorresteijn [22] measured a value of 1.65 for h_{TP}/h_L. The following example calculation illustrates the use of the general two-phase heat transfer correlation, Eq. (23), to predict the h_{TP}/h_L value measured by Dorresteijn [22].

From the measured superficial gas and liquid velocities, and void fraction, the gas and liquid velocities are found to be

$$V_G = \frac{V_{SG}}{\alpha} = 11.9\,\text{m/s} \text{ and } V_L = \frac{V_{SL}}{1-\alpha} = 9.58\,\text{m/s}$$

The gas and liquid mass flow rates are calculated as

$$\dot{m}_G = \rho_G V_{SG} A = 0.0771 \text{ kg/s} \text{ and}$$

$$\dot{m}_L = \rho_L V_{SL} A = 10.2 \text{ kg/s}$$

Using the gas and liquid mass flow rates, the quality is determined to be

$$x = \frac{\dot{m}_G}{\dot{m}_G + \dot{m}_L} = 0.0075$$

Equations (17) and (16) are then used for calculating the flow pattern factor (F_p):

$$F_S = \frac{2}{\pi}\tan^{-1}\left(\sqrt{\frac{\rho_G (V_G - V_L)^2}{g D (\rho_L - \rho_G)}}\right) = 0.0969 \quad \text{and}$$

$$F_P = (1-\alpha) + \alpha F_S^2 = 0.336$$

Using Eqs. (22) and (21), the inclination factor (I^*) for vertical tube ($\theta = 90^\circ$) is calculated to be

$$Eo = \frac{(\rho_L - \rho_G) g D^2}{\sigma} = 1600 \text{ and } I^* = 1 + Eo\,|\sin\theta| = 1601$$

The surface tension (σ) of gas–oil is assumed to be 25 N/m, since the surface tension for live gas–oil at 1380 kPa ranges from 20 to 30 N/m [66]. Using the general two-phase heat transfer correlation, Eq. (23), the value for h_{TP}/h_L is estimated to be

$$\frac{h_{TP}}{h_L} = F_P\left[1 + 0.55\left(\frac{x}{1-x}\right)^{0.1}\left(\frac{1-F_P}{F_P}\right)^{0.4} \times \left(\frac{Pr_G}{Pr_L}\right)^{0.25}\left(\frac{\mu_L}{\mu_G}\right)^{0.25}(I^*)^{0.25}\right] = 1.53$$

The Prandtl number (Pr_G) and dynamic viscosity (μ_G) for air are 0.71 and 18.2×10^{-6} Pa·s, respectively. Comparing with the measured value of $h_{TP}/h_L = 1.65$ by Dorresteijn [22], the general two-phase heat transfer correlation, Eq. (23), underpredicted the measured value by 7.3%.

Application in Air and Silicone Flow

Liquid silicone such as Dow Corning 200 Fluid, 5 cs, is used primarily as an ingredient in cosmetic and personal care products due to its high spreadability, low surface tension ($\sigma = 19.7$ N/m), nongreasy, soft feel, and subtle skin lubricity characteristics. A two-phase flow of air and silicone (Dow Corning 200 Fluid, 5 cs) with $\dot{m}_L = 0.907$ kg/s, $x = 2.08 \times 10^{-5}$, $\rho_G = 1.19$ kg/m^3, $\rho_L = 913$ kg/m^3, $\mu_G = 18.4 \times 10^{-6}$ Pa-s, $\mu_L = 45.7 \times 10^{-4}$ Pa-s, $\mu_W = 39.8 \times 10^{-4}$ Pa-s, $Pr_G = 0.71$, $Pr_L = 64$, $k_L = 0.117$ W/(m-K), and $\alpha = 0.011$ flows inside an 11.7-mm-diameter vertical ($\theta = 90^\circ$) tube. Using the general two-phase heat transfer correlation, Eq. (23), the two-phase heat transfer coefficient for this flow can be estimated.

With known liquid mass flow rate ($\dot{m}_L$) and quality (x), the gas mass flow rate ($\dot{m}_G$) is determined using

$$\dot{m}_G = \frac{x}{1-x}\dot{m}_L = 1.89 \times 10^{-5} \text{ kg/s}$$

From the gas and liquid mass flow rates, the superficial gas and liquid velocities can be calculated:

$$V_{SG} = \frac{\dot{m}_G}{\rho_G A} = 0.149 \text{ m/s and } V_{SL} = \frac{\dot{m}_L}{\rho_L A} = 9.24 \text{ m/s}$$

Using the superficial velocities and void fraction, the gas and liquid velocities are found to be

$$V_G = \frac{V_{SG}}{\alpha} = 13.5 \text{ m/s and } V_L = \frac{V_{SL}}{1-\alpha} = 9.34 \text{ m/s}$$

Equations (17) and (16) are then used for calculating the flow pattern factor (F_p):

$$F_S = \frac{2}{\pi}\tan^{-1}\left(\sqrt{\frac{\rho_G (V_G - V_L)^2}{g D (\rho_L - \rho_G)}}\right) = 0.266 \text{ and}$$

$$F_P = (1-\alpha) + \alpha F_S^2 = 0.990$$

Using Eqs. (22) and (21), the inclination factor (I^*) for vertical tube ($\theta = 90^\circ$) is calculated to be

$$Eo = \frac{(\rho_L - \rho_G) g D^2}{\sigma} = 62.1 \text{ and } I^* = 1 + Eo\,|\sin\theta| = 63.1$$

Finally, with the general two-phase heat transfer correlation, Eq. (23), the value for h_{TP} is estimated to be

$$h_{TP} = h_L F_P \left[1 + 0.55\left(\frac{x}{1-x}\right)^{0.1}\left(\frac{1-F_P}{F_P}\right)^{0.4} \times \left(\frac{Pr_G}{Pr_L}\right)^{0.25}\left(\frac{\mu_L}{\mu_G}\right)^{0.25}(I^*)^{0.25}\right] = 3550 \text{ W/m}^2\text{K}$$

When compared with the measured two-phase heat transfer coefficient of 3480 W/(m^2-K) by Rezkallah [13] in similar flow conditions, the general two-phase heat transfer correlation, Eq. (23), overpredicted the measured value by 2%.

Application in Microgravity Condition

An air–water slug flow heat transfer coefficient in microgravity condition (less than 1% of earth's normal gravity) was measured by Witte et al. [67] in a 25.4-mm-diameter horizontal tube. In the conditions at which $V_{SG} = 0.3$ m/s, $V_{SL} = 0.544$ m/s, $\rho_G = 1.16$ kg/m^3, $\rho_L = 997$ kg/m^3, $\mu_G = 18.5 \times 10^{-6}$ Pa-s, $\mu_L = 85.5 \times 10^{-5}$ Pa-s, $\mu_W = 73.9 \times 10^{-5}$ Pa-s, $Pr_G = 0.71$, $Pr_L = 5.0$, $k_L = 0.613$ W/(m-K), and $\alpha = 0.27$, Witte et al. [67] measured a value of 3169 W/(m^2-K) for the two-phase heat transfer coefficient (h_{TP}). The following example calculation illustrates the use of the general two-phase heat transfer correlation, Eq. (23), to predict the h_{TP} value measured by Witte et al. [67].

From the measured superficial gas and liquid velocities, and void fraction, the gas and liquid velocities are found to be

$$V_G = \frac{V_{SG}}{\alpha} = 1.11 \text{ m/s and } V_L = \frac{V_{SL}}{1-\alpha} = 0.745 \text{ m/s}$$

The gas and liquid mass flow rates are calculated as

$$\dot{m}_G = \rho_G V_{SG} A = 1.76 \times 10^{-4} \text{ kg/s} \quad \text{and}$$

$$\dot{m}_L = \rho_L V_{SL} A = 0.275 \text{ kg/s}$$

Using the gas and liquid mass flow rates, the quality is determined to be

$$x = \frac{\dot{m}_G}{\dot{m}_G + \dot{m}_L} = 6.40 \times 10^{-4}$$

Equations (17) and (16) are then used for calculating the flow pattern factor (F_p):

$$F_S = \frac{2}{\pi}\tan^{-1}\left(\sqrt{\frac{\rho_G (V_G - V_L)^2}{g D (\rho_L - \rho_G)}}\right) = 0.0159 \quad \text{and}$$

$$F_P = (1-\alpha) + \alpha F_S^2 = 0.730$$

The inclination factor (I^*) has a value of one in horizontal tube ($\theta = 0$). Thus, using the general two-phase heat transfer correlation, Eq. (23), the value for h_{TP} is estimated to be

$$h_{TP} = h_L F_P \left[1 + 0.55\left(\frac{x}{1-x}\right)^{0.1}\left(\frac{1-F_P}{F_P}\right)^{0.4}\left(\frac{Pr_G}{Pr_L}\right)^{0.25} \times \left(\frac{\mu_L}{\mu_G}\right)^{0.25}(I^*)^{0.25}\right] = 2810 \text{ W/m}^2\text{K}$$

Comparing with the measured two-phase heat transfer coefficient of 3169 W/(m^2-K) by Witte et al. [67], the general two-phase heat transfer correlation, Eq. (23), underpredicted the measured value by 11%. Although the preceding example showed that Eq. (23) can satisfactorily estimate heat transfer coefficient for one case of two-phase flow under reduced gravity condition, it should be noted that Eq. (23) was not developed to handle reduced gravity conditions. Validation with experimental results needs to be done before the use of Eq. (23) in reduced gravity conditions can be recommended.

SUMMARY

The work documented in this article initiated with the motivation to understand, in both fundamentals and industrial applications, the importance of non-boiling two-phase flow heat transfer in pipes. Through the survey of literature and tracing the validity and limitations of the numerous two-phase non-boiling heat transfer correlations that have been published over the past 50 years, it was established that there is no single correlation capable of predicting the two-phase flow heat transfer for all fluid combinations in vertical pipes [11].

The results from the literature survey prompted the development of a two-phase non-boiling heat transfer correlation that is robust and applicable to turbulent gas–liquid flow in vertical pipes with different flow patterns and fluid combinations [36].

Since the development of the two-phase non-boiling heat transfer correlation for vertical pipes by Kim et al. [36], extensive efforts have been invested in the development of the general two-phase heat transfer correlation, Eq. (23). When compared with experimental data from horizontal, slightly inclined, and vertical pipes with various fluid combinations and flow patterns, the general two-phase heat transfer correlation successfully predicted 90% of the data points within ±25% agreement with the experimental data and has a root-mean-square deviation of 18.4% from the experimental data. In addition, practical illustrations of using the general two-phase heat transfer correlation were also discussed.

In the efforts of investigating non-boiling two-phase flow heat transfer in pipes, a significant amount of work has also been done on understanding void fraction. A very extensive comparison of 68 void fraction correlations available in the literature against 2845 experimental data points was conducted by Woldesemayat and Ghajar [41]. From this work an improved void fraction correlation, Eq. (20), was proposed. The improved void fraction correlation gives noticeable improvements over other correlations when compared with 2845 experimental data points of various pipe sizes, inclinations, and two-phase fluid mixtures from various sources with different experimental facilities.

FUTURE PLANS

As pointed out in the introduction, the overall objective of our research has been to develop a heat transfer correlation that is robust enough to span all or most of the fluid combinations, flow patterns, flow regimes, and pipe orientations (vertical, inclined, and horizontal). As presented in this article, we have made a lot of progress toward this goal. However, we still have a long way to go. In order to accomplish our research objective, we need to have a much better understanding of the heat transfer mechanism in each flow pattern and perform systematic heat transfer measurements to capture the effect of several parameters that influence the heat transfer results. We will complement these measurements with extensive flow visualizations.

We also plan to take systematic isothermal pressure drop measurements in the same regions where we will obtain or have obtained heat transfer data. We will then use the pressure drop data through "modified Reynolds analogy" to back out heat transfer data. By comparing the predicted heat transfer results against our experimental heat transfer results, we would be able to establish the correct form of the "modified Reynolds analogy." Once the correct relationship has been established, it will be used to obtain two-phase heat transfer data for the regions where, due to limitations of our experimental setup, we did not collect heat transfer data. The additional task at this stage would be collection of isothermal pressure drop in these regions.

At the present stage, the general two-phase heat transfer correlation, Eq. (23), has been validated with experimental data for horizontal, slightly inclined, and vertical pipes; however, its performance for pipe inclination angles between 7° and 90° has yet to be validated. Hence, we have recently constructed a robust experimental setup that is equipped for measuring heat transfer, pressure drop, and void fraction and also conducting flow visualization in air–water flow for all major flow patterns and inclination angles from 0° (horizontal) to ±90° (vertical). A comparison between the capabilities of the current and new experimental setups is summarized in Table 11.

Table 11 Comparison of capabilities of the current and new experimental setups

Capability	Current experimental setup	New experimental setup
Test section I.D.	2.54 cm (1 inch)	1.27 cm (0.5 inch)
Heat transfer section with flow observation sections	Yes	Yes
Heat transfer section for pressure drop measurement	Yes	Yes
Heat transfer section for heat transfer measurement	Yes	Yes
Isothermal section for flow visualization	No	Yes
Isothermal section for pressure drop measurement	No	Yes
Isothermal section for void fraction measurement	No	Yes
Test section orientation	0° to 7°	0° to ±90°

The new experimental setup consists of two test sections. One test section is a stainless-steel pipe and will be used for heat transfer and heated pressure drop measurements. The other test section is a clear polycarbonate pipe and will be used for isothermal pressure drop and void fraction measurements and flow visualization. The capabilities of the new experimental setup allow an undertaking that combines the study of heat transfer, flow patterns, pressure drop, void fraction, and inclination effects. Such combination of study has not been documented yet.

The already-mentioned systematic measurements will allow us to develop a complete database for the development of our "general" two-phase heat transfer correlation.

NOMENCLATURE

A	cross-sectional area, m^2
C	constant value of the leading coefficient in Eqs. (11), (19), and (23), dimensionless
C_0	distribution parameter, dimensionless
c	specific heat at constant pressure, kJ/(kg-K)
D	pipe inside diameter, m
Eo	Eötvös number, dimensionless
F_P	flow pattern factor, Eq. (16), dimensionless
F_S	shape factor, Eq. (17), dimensionless
G_t	mass velocity of total flow, ρV, kg/(s-m^2)
g	gravitational acceleration, m/s^2
h	heat transfer coefficient, W/(m^2-K)
I	inclination factor, Eq. (18), dimensionless

I^*	modified inclination factor, Eq. (21), dimensionless
K	slip ratio, dimensionless
k	thermal conductivity, W/(m-K)
L	length, m
m	exponent on the quality ratio term in Eqs. (11), (19), and (23), dimensionless
$\dot{m}$	mass flow rate, kg/s or kg/min
Nu	Nusselt number, hD/k, dimensionless
N_{ST}	number of thermocouple stations, Eq. (25), dimensionless
n	exponent in Eqs. (11), (19), and (23), dimensionless
P	mean system pressure, Pa
Pa	atmospheric pressure, Pa
ΔP	pressure drop, Pa
$\Delta P/\Delta L$	total pressure drop per unit length, Pa/m
p	exponent on the Prandtl number ratio term in Eqs. (11), (19), and (23), dimensionless
Pr	Prandtl number, $c\mu/k$, dimensionless
Q	volumetric flow rate, m^3/s
q	exponent on the viscosity ratio term in Eqs. (11), (19), and (23), dimensionless
$\dot{q}''$	heat flux, W/m^2
r	exponent on the inclination factor in Eqs. (19), and (23), dimensionless
Re	Reynolds number, $\rho VD/\mu_B$, dimensionless
Re_L	liquid in-situ Reynolds number, $4\dot{m}/(\pi \mu_L D\sqrt{1-\alpha})$, dimensionless
Re_M	mixture Reynolds number, dimensionless
Re_{TP}	two-phase flow Reynolds number, dimensionless
R_L	liquid holdup, $1-\alpha$, dimensionless
S_L	wetted perimeter, m
T	temperature, K
u_{GM}	drift velocity for gas, m/s
V	mean velocity, m/s
X_{TT}	Martinelli parameter, dimensionless
x	flow quality, $\dot{m}_G/(\dot{m}_G+\dot{m}_L)$, dimensionless
z	axial coordinate, Eq. (25), m
Δz	element length of each thermocouple station, Eq. (25), m

Greek Symbols

α	void fraction, $A_G/(A_G+A_L)$, dimensionless
μ	dynamic viscosity, Pa-s
ν	kinematic viscosity, m^2/s
ρ	density, kg/m^3
σ	surface tension, N/m
θ	inclination angle, radians

Subscripts

atm	atmosphere
B	bulk
CAL	calculated
EXP	experimental
eff	effective
eq	equilibrium state
G	gas
k	index of thermocouple station, Eq. (25)
L	liquid
SG	superficial gas
SL	superficial liquid
sys	system
TP	two-phase
TPF	two-phase frictional
W	wall

Superscripts

–	local mean
~	nondimensionalized

REFERENCES

[1] Shiu, K. C., and Beggs, H. D., Predicting Temperatures in Flowing Oil Wells, *Journal of Energy Resources Technology,* vol. 102, no. 1, pp. 2–11, 1980.

[2] Trevisan, O. V., Franca, F. A., and Lisboa, A. C., Oil Production in Offshore Fields: An Overview of the Brazilian Technology Development Program, *Proceedings of the 1st World Heavy Oil Conference*, Beijing, China, Paper No. 2006–437, November 13–15, 2006.

[3] Furuholt, E. M., Multiphase Technology: Is It of Interest for Future Field Developments?, *Society of Petroleum Engineers European Petroleum Conference*, London, England, Paper No. 18361, October 17–19, 1988.

[4] McClaflin, G. G., and Whitfill, D. L., Control of Paraffin Deposition in Production Operations, *Journal of Petroleum Technology,* vol. 36, no. 12, pp. 1965–1970, 1984.

[5] Fogler, H. S., *Paraffin Research,* Porous Media Research Group, sitemaker.umich.edu/sfogler/paraffin_deposition, retrieved November 25, 2008.

[6] Singh, P., Venkatesan, R., Fogler, H. S., and Nagarajan, N., Formation and Aging of Incipient Thin Film Wax–Oil Gels, *AIChE Journal,* vol. 46, no. 5, pp. 1059–1074, 2000.

[7] Celata, G. P., Chiaradia, A., Cumo, M., and D'Annibale, F., Heat Transfer Enhancement by Air Injection in Upward Heated Mixed-Convection Flow of Water, *International Journal of Multiphase Flow,* vol. 25, pp. 1033–1052, 1999.

[8] Fore, L. B., Witte, L. C., and McQuillen, J. B., Heat Transfer to Annular Gas–Liquid Mixtures at Reduced Gravity, *Journal of Thermophysics and Heat Transfer,* vol. 10, no. 4, pp. 633–639, 1996.

[9] Fore, L. B., Witte, L. C., and McQuillen, J. B., Heat Transfer to Two-Phase Slug Flows Under Reduced-Gravity Conditions, *International Journal of Multiphase Flow,* vol. 23, no. 2, pp. 301–311, 1997.

[10] Wang, L., Huang, X.-H., and Lu, Z., Immiscible Two-Component Two-Phase Gas–Liquid Heat Transfer on Shell Side of a TEMA-F

Heat Exchanger, *Heat and Mass Transfer,* vol. 40, pp. 301–306, 2004.

[11] Kim, D., Ghajar, A. J., Dougherty, R. L., and Ryali, V. K., Comparison of 20 Two-Phase Heat Transfer Correlations With Seven Sets of Experimental Data, Including Flow Pattern and Tube Inclination Effects, *Heat Transfer Engineering,* vol. 20, no. 1, pp. 15–40, 1999.

[12] Vijay, M. M., *A Study of Heat Transfer in Two-Phase Two-Component Flow in a Vertical Tube*, Ph.D. Thesis, University of Manitoba, Winnipeg, Manitoba, Canada, 1978.

[13] Rezkallah, K. S., *Heat Transfer and Hydrodynamics in Two-Phase Two-Component Flow in a Vertical Tube*, Ph.D. Thesis, University of Manitoba, Winnipeg, Manitoba, Canada, 1987.

[14] Aggour, M. A., *Hydrodynamics and Heat Transfer in Two-Phase Two-Component Flow*, Ph.D. Thesis, University of Manitoba, Winnipeg, Manitoba, Canada, 1978.

[15] Pletcher, R. H., *An Experimental and Analytical Study of Heat Transfer and Pressure Drop in Horizontal Annular Two-Phase, Two-Component Flow*, Ph.D. Thesis, Cornell University, Ithaca, NY, 1966.

[16] King, C. D. G., *Heat Transfer and Pressure Drop for an Air–Water Mixture Flowing in a 0.737inch I.D. Horizontal Tube*, M.S. Thesis, University of California, Berkeley, 1952.

[17] Knott, R. F., Anderson, R. N., Acrivos, A., and Petersen, E. E., An Experimental Study of Heat Transfer to Nitrogen–Oil Mixtures, *Industrial & Engineering Chemistry,* vol. 51, no. 11, pp. 1369–1372, 1959.

[18] Chu, Y.-C., and Jones, B. G., Convective Heat Transfer Coefficient Studies in Upward and Downward, Vertical, Two-Phase, Non-Boiling Flows, *AIChE Symposium Series,* vol. 76, no. 199, pp. 79–90, 1980.

[19] Kudirka, A. A., Grosh, R. J., and McFadden, P. W., Heat Transfer in Two-Phase Flow of Gas–Liquid Mixtures, *Industrial & Engineering Chemistry Fundamentals,* vol. 4, no. 3, pp. 339–344, 1965.

[20] Davis, E. J., and David, M. M., Two-Phase Gas–Liquid Convection Heat Transfer, *Industrial & Engineering Chemistry Fundamentals,* vol. 3, no. 2, pp. 111–118, 1964.

[21] Martin, B. W., and Sims, G. E., Forced Convection Heat Transfer to Water With Air Injection in a Rectangular Duct, *International Journal of Heat and Mass Transfer,* vol. 14, no. 8, pp. 1115–1134, 1971.

[22] Dorresteijn, W. R., Experimental Study of Heat Transfer in Upward and Downward Two-Phase Flow of Air and Oil Through 70-mm Tubes, *Proceedings of the 4th International Heat Transfer Conference*, Paris & Versailles, France, vol. 5, B5.9, 1970.

[23] Oliver, D. R., and Wright, S. J., Pressure Drop and Heat Transfer in Gas–Liquid Slug Flow in Horizontal Tubes, *British Chemical Engineering,* vol. 9, pp. 590–596, 1964.

[24] Dusseau, W. T., *Overall Heat Transfer Coefficient for Air–Water Froth in a Vertical Pipe,* M.S. Thesis, Vanderbilt University, Nashville, TN, 1968.

[25] Ravipudi, S. R., and Godbold, T. M., The Effect of Mass Transfer on Heat Transfer on Heat Transfer Rates for Two-Phase Flow in a Vertical Pipe, *Proceedings of the 6th International Heat Transfer Conference*, Toronto, Canada, vol. 1, pp. 505–510, 1978.

[26] Elamvaluthi, G., and Srinivas, N. S., Two-Phase Heat Transfer in Two Component Vertical Flows, *International Journal of Multiphase Flow,* vol. 10, no. 2, pp. 237–242, 1984.

[27] Rezkallah, K. S., and Sims, G. E., Examination of Correlations of Mean Heat Transfer Coefficients in Two-Phase Two-Component Flow in Vertical Tubes, *AIChE Symposium Series,* vol. 83, no. 257, pp. 109–114, 1987.

[28] Groothuis, H., and Hendal, W. P., Heat Transfer in Two-Phase Flow, *Chemical Engineering Science,* vol. 11, pp. 212–220, 1959.

[29] Serizawa, A., Kataoka, I., and Michiyoshi, I., Turbulence Structure of Air–Water Bubbly Flow—III. Transport Properties, *International Journal of Multiphase Flow,* vol. 2, pp. 247–259, 1975.

[30] Hughmark, G. A., Holdup and Heat Transfer in Horizontal Slug Gas–Liquid Flow, *Chemical Engineering Science,* vol. 20, pp. 1007–1010, 1965.

[31] Shah, M. M., Generalized Prediction of Heat Transfer during Two Component Gas–Liquid Flow in Tubes and Other Channels, *AIChE Symposium Series,* vol. 77, no. 208, pp. 140–151, 1981.

[32] Khoze, A. N., Dunayev, S. V., and Sparin, V. A., Heat and Mass Transfer in Rising Two-Phase Flows in Rectangular Channels, *Heat Transfer Soviet Research,* vol. 8, no. 3, pp. 87–90, 1976.

[33] Ueda, T., and Hanaoka, M., On Upward Flow of Gas–Liquid Mixtures in Vertical Tubes: 3rd Report, Heat Transfer Results and Analysis, *Bulletin of JSME,* vol. 10, no. 42, pp. 1008–1015, 1967.

[34] Vijay, M. M., Aggour, M. A., and Sims, G. E., A Correlation of Mean Heat Transfer Coefficients for Two-Phase Two-Component Flow in a Vertical Tube, *Proceedings of the 7th International Heat Transfer Conference*, Munich, vol. 5, pp. 367–372, 1982.

[35] Sieder, E. N., and Tate, G. E., Heat Transfer and Pressure Drop of Liquids in Tubes, *Industrial & Engineering Chemistry,* vol. 28, no. 12, pp. 1429–1435, 1936.

[36] Kim, D., Ghajar, A. J., and Dougherty, R. L., Robust Heat Transfer Correlation for Turbulent Gas–Liquid Flow in Vertical Pipes, *Journal of Thermophysics and Heat Transfer,* vol. 14, no. 4, pp. 574–578, 2000.

[37] Chisholm, D., Research Note: Void Fraction During Two-Phase Flow, *Journal of Mechanical Engineering Science,* vol. 15, no. 3, pp. 235–236, 1973.

[38] Ghajar, A. J., and Kim, J., A Non-Boiling Two-Phase Flow Heat Transfer Correlation for Different Flow Patterns and Pipe Inclination Angles, *Proceedings of the 2005 ASME Summer Heat Transfer Conference*, San Francisco, CA, Paper No. HT2005–72078, July 17–22, 2005.

[39] Kim, J., and Ghajar, A. J., A General Heat Transfer Correlation for Non-Boiling Gas–Liquid Flow With Different Flow Patterns in Horizontal Pipes, *International Journal of Multiphase Flow,* vol. 32, no. 4, pp. 447–465, 2006.

[40] Ghajar, A. J., and Tang, C. C., Heat Transfer Measurements, Flow Pattern Maps and Flow Visualization for Non-Boiling Two-Phase Flow in Horizontal and Slightly Inclined Pipe, *Heat Transfer Engineering,* vol. 28, no. 6, pp. 525–540, 2007.

[41] Woldesemayat, M. A., and Ghajar, A. J., Comparison of Void Fraction Correlations for Different Flow Patterns in Horizontal and Upward Inclined Pipes, *International Journal of Multiphase Flow,* vol. 33, pp. 347–370, 2007.

[42] Tang, C. C., and Ghajar, A. J., Validation of a General Heat Transfer Correlation for Non-Boiling Two-Phase Flow with Different Flow Patterns and Pipe Inclination Angles, *Proceedings of the 2007 ASME-JSME Thermal Engineering Summer Heat Transfer Conference*, Vancouver, BC, Canada, Paper No. HT2007–32219, July 8–12, 2007.

[43] Ghajar, A. J., Kim, J., and Tang, C., Two-Phase Flow Heat Transfer Measurements and Correlation for the Entire Flow Map in Horizontal Pipes, *Proceedings of the 13th International Heat Transfer Conference*, Sydney, Australia, Paper No. MPH-14, August 13–18, 2006.

[44] Eaton, B. A., *The Prediction of Flow Patterns, Liquid Holdup and Pressure Losses Occurring during Continuous Two-Phase Flow in Horizontal Pipelines*, Ph.D. Thesis, University of Texas, Austin, 1966.

[45] Beggs, H. D., *An Experimental Study of Two Phase Flow in Inclined Pipes*, Ph.D. Thesis, University of Tulsa, Tulsa, 1972.

[46] Spedding, P. L., and Nguyen, V. T., *Data on Holdup, Pressure Loss and Flow Patterns for Two-Phase Air–Water Flow in an Inclined Pipe,* University of Auckland, Auckland, New Zealand, Engineering Report 122, 1976.

[47] Mukherjee, H., *An Experimental Study of Inclined Two-Phase Flow*, Ph.D. Thesis, University of Tulsa, Tulsa, Oklahoma, 1979.

[48] Minami, K., and Brill, J. P., Liquid Holdup in Wet-Gas Pipelines, *SPE Production Engineering,* vol. 2, no. 1, pp. 36–44, 1987.

[49] Franca, F., and Lahey, R. T., Jr., The Use of Drift-Flux Techniques for the Analysis of Horizontal Two-Phase Flows, *International Journal of Multiphase Flow,* vol. 18, no. 6, pp. 787–801, 1992.

[50] Abdul-Majeed, G. H., Liquid Holdup in Horizontal Two-Phase Gas–Liquid Flow, *Journal of Petroleum Science and Engineering,* vol. 15, pp. 271–280, 1996.

[51] Sujumnong, M., *Heat Transfer, Pressure Drop and Void Fraction in Two-Phase, Two Component Flow in a Vertical Tube*, Ph.D. Thesis, University of Manitoba, Winnipeg, Manitoba, Canada, 1998.

[52] Morooka, S., Ishizuka, T., IIzuka, M., and Yoshimura, K., Experimental Study on Void Fraction in a Simulated BWR Fuel Assembly (Evaluation of Cross-Sectional Averaged Void Fraction), *Nuclear Engineering and Design,* vol. 114, pp. 91–98, 1989.

[53] Dix, G. E., *Vapor Void Fractions for Forced Convection with Subcooled Boiling at Low Flow Rates*, Ph.D. Thesis, University of California, Berkeley, 1971.

[54] Rouhani, S. Z., and Axelsson, E., Calculation of Void Volume Fraction in the Subcooled and Quality Boiling Regions, *International Journal of Heat and Mass Transfer,* vol. 13, no. 2, pp. 383–393, 1970.

[55] Hughmark, G. A., Holdup in Gas–Liquid Flow, *Chemical Engineering Progress,* vol. 58, no. 4, pp. 62–65, 1962.

[56] Premoli, A., Francesco, D., and Prima, A., An Empirical Correlation for Evaluating Two-Phase Mixture Density under Adiabatic Conditions, *European Two-Phase Flow Group Meeting*, Milan, Italy, 1970.

[57] Filimonov, A. I., Przhizhalovski, M. M., Dik, E. P., and Petrova, J. N., The Driving Head in Pipes With a Free Interface in the Pressure Range from 17 to 180 atm, *Teploenergetika,* vol. 4, no. 10, pp. 22–26, 1957.

[58] Ghajar, A. J., and Kim, J., Calculation of Local Inside-Wall Convective Heat Transfer Parameters from Measurements of Local Outside-Wall Temperatures Along an Electrically Heated Circular Tube, in *Heat Transfer Calculations*, ed. M. Kutz, pp. 23.3–23.27, McGraw-Hill, New York, 2006.

[59] Kim, D., and Ghajar, A. J., Heat Transfer Measurements and Correlations for Air–Water Flow of Different Flow Patterns in a Horizontal Pipe, *Experimental Thermal and Fluid Science,* vol. 25, no. 8, pp. 659–676, 2002.

[60] Durant, W. B., *Heat Transfer Measurement of Annular Two-Phase Flow in Horizontal and a Slightly Upward Inclined Tube*, M.S. Thesis, Oklahoma State University, Stillwater, 2003.

[61] Kline, S. J., and McClintock, F. A., Describing Uncertainties in Single-Sample Experiments, *Mechanical Engineering,* vol. 75, no. 1, pp. 3–8, 1953.

[62] Taitel, Y., and Dukler, A. E., A Model for Predicting Flow Regime Transitions in Horizontal and Near Horizontal Gas–Liquid Flow, *AIChE Journal,* vol. 22, no. 1, pp. 47–55, 1976.

[63] Barnea, D., Shoham, O., Taitel, Y., and Dukler, A. E., Flow Pattern Transition for Gas–Liquid Flow in Horizontal and Inclined Pipes. Comparison of Experimental Data With Theory, *International Journal of Multiphase Flow,* vol. 6, pp. 217–225, 1980.

[64] Mandhane, J. M., Gregory, G. A., and Aziz, K., A Flow Pattern Map for Gas–Liquid Flow in Horizontal Pipes, *International Journal of Multiphase Flow,* vol. 1, pp. 537–553, 1974.

[65] Franca, F. A., Bannwart, A. C., Camargo, R. M. T., and Gonçalves, M. A. L., Mechanistic Modeling of the Convective Heat Transfer Coefficient in Gas–Liquid Intermittent Flows, *Heat Transfer Engineering,* vol. 29, no. 12, pp. 984–998, 2008.

[66] Abdul-Majeed, G. H., and Abu Al-Soof, N. B., Estimation of Gas–Oil Surface Tension, *Journal of Petroleum Science and Engineering,* vol. 27, pp. 197–200, 2000.

[67] Witte, L. C., Bousman, W. S., and Fore, L. B., *Studies of Two-Phase Flow Dynamics and Heat Transfer at Reduced Gravity Conditions*, NASA Lewis Research Center, Cleveland, OH, NASA Contractor Report 198459, 1996.

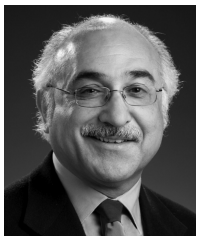

Afshin J. Ghajar is a Regents Professor and Director of Graduate Studies in the School of Mechanical and Aerospace Engineering at Oklahoma State University Stillwater, and a Honorary Professor of Xi'an Jiaotong University, Xi'an, China. He received his B.S., M.S., and Ph.D. all in mechanical engineering from Oklahoma State University. His expertise is in experimental and computational heat transfer and fluid mechanics. Dr. Ghajar has been a summer research fellow at Wright Patterson AFB (Dayton, OH) and Dow Chemical Company (Freeport, TX). He and his co-workers have published over 150 reviewed research papers. He has received several outstanding teaching/service awards, such as the Regents Distinguished Teaching Award; Halliburton Excellent Teaching Award; Mechanical Engineering Outstanding Faculty Award for Excellence in Teaching and Research; Golden Torch Faculty Award for Outstanding Scholarship, Leadership, and Service by the Oklahoma State University/National Mortar Board Honor Society; and recently the College of Engineering Outstanding Advisor Award. Dr. Ghajar is a fellow of the American Society of Mechanical Engineers (ASME), *Heat Transfer Series Editor* for Taylor & Francis/CRC Press, and editor-in-chief of *Heat Transfer Engineering*. He is also the co-author of the fourth edition of Cengel and Ghajar, *Heat and Mass Transfer—Fundamentals and Applications*, McGraw-Hill, 2010.

Clement C. Tang is a Ph.D. candidate in the School of Mechanical and Aerospace Engineering at Oklahoma State University, Stillwater. He received his B.S. and M.S. degrees in mechanical engineering from Oklahoma State University. His areas of specialty are single-phase flow in mini and microtubes and two-phase flow heat transfer.